Involvement of 3D osteoblast migration and bone apatite during in vitro early osteocytogenesis

Marc Robin, Claudia Almeida, Thierry Azaïs, Bernard Haye, Corinne Illoul, Julie Lesieur, Marie-Madeleine Giraud-Guille, Nadine Nassif, Christophe Hélary

Involvement of 3D osteoblast migration and bone apatite during *in vitro* early osteocytogenesis

Marc Robin[a], Claudia Almeida[a], Thierry Azaïs[a], Bernard Haye[a], Corinne Illoul[a], Julie Lesieur[b], Marie-Madeleine Giraud-Guille[a], Nadine Nassif[a,*], Christophe Hélary[a,*]

[a] *Sorbonne Universités UPMC Univ Paris 06, CNRS, Collège de France, Laboratoire Chimie de la Matière Condensée de Paris UMR 7574, 11 place Marcelin Berthelot 75005 Paris, France*

[b] *EA 2496, Pathologies, Imaging and Biotherapies of the Tooth, UFR Odontologie, University Paris Descartes PRES Sorbonne Paris Cite, Montrouge, France*

Corresponding authors: nadine.nassif@upmc.fr ; christophe.helary@upmc.fr

The transition from osteoblast to osteocyte is described to occur through passive entrapment mechanism (self-buried, or embedded by neighboring cells). Here, we provide evidence of a new pathway where osteoblasts are "more" active than generally assumed. We demonstrate that osteoblasts possess the ability to migrate and differentiate into early osteocytes inside dense collagen matrices. This step involves *MMP-13* simultaneously with *IBSP* and *DMP1* expression. We also show that osteoblast migration is enhanced by the presence of apatite bone mineral. To reach this conclusion, we used an *in vitro* hybrid model based on both the structural characteristics of the osteoid tissue (including its density, texture and three-dimensional order), and the use of bone-like apatite. This finding highlights the mutual dynamic influence of osteoblast cell and bone extra cellular matrix. Such interactivity extends the role of physicochemical effects in bone morphogenesis complementing the widely studied molecular signals. This result represents a conceptual advancement in the fundamental understanding of bone formation.

1. Introduction

Osteoblasts are the main cells responsible for bone matrix production through a regulated spatio-temporal sequence. Up to eight recognizable transitional steps are proposed in the literature and the kinetic of differentiation into osteocytes includes different maturation stages that can be morphologically and biochemically recognized[1-3]. Osteoblasts are described as bordering cells along the bone trabecula. When they are entrapped in the bone extracellular matrix (ECM) they produced, *i.e.* the osteoid tissue, they differentiate into osteocytes[3]. Osteoid tissue is defined as a soft unmineralized tissue mainly composed of ECM proteins, mostly fibrillar type I collagen that serves as a substrate for the bone remodeling process[4]. While the molecular pathways (gene expression and protein production) of the osteocytic differentiation are familiar, the microenvironment and the related physico-chemical conditions that trigger this differentiation remain elusive. Recent work highlights the dynamic nature of the bone tissue expanding the function played by each type of cells and, in particular, the key role of the osteoblast motility on the bone surface[1]. Different factors are identified as directing the osteoblast behavior. Among these, a low oxygen tension is understood to promote the osteoblastic differentiation[5] and the presence of mechanical stress is described to modulate the osteoblast proliferation[6] and phenotype[7, 8]. Additionally, the fibrillar feature of the collagen network appears crucial since it allows the osteoblasts adhesion *via* integrin α1β1 and α2β1[9, 10], favors the physiological-type shape and directs cells toward osteoblast maturation by changing the local topography[11]. At a larger scale, the collagen network density prevents cell apoptosis and promotes osteoblast differentiation[12, 13].

Dense fibrillar collagen matrices have been developed with the aim of mimicking the composition and the structure of native osteoid tissue. Thanks to their composition (type I collagen), texture (fibrils) and density (40 mg/mL), these matrices were proposed as a connective tissue model for cell culture[14]. They provide an appropriate three dimensional (3D) microenvironment for the adhesion, spreading and differentiation of osteoblasts[11, 15], for the investigation of the role of non-collagenous proteins (NCPs) in the mineralization process[13] or the study of the osteoblast behavior in a bone healing context[16].
In the present study, the model was adapted to simulate the first events of the osteoblast-to-osteocyte transition. For this purpose, synthetic apatite platelets with structure and properties mimicking the biological ones[17] were precipitated within the collagen matrix offering a transient tissue model to investigate a putative role of the mineral content on the osteoblast behavior.

Here, in addition to the "passive" entrapment event (*i.e.* self-burial or embedment by neighboring cells), we provide evidence for an active mechanism in which osteoblasts migrate. This pathway involves the Matrix Metalloproteinase 13 (*MMP-13)* concomitantly with their differentiation into mineralizing osteocytes and the expression of the integrin-binding sialoprotein (*IBSP)*. Additionally, we show that this property is further stimulated by bone-like apatite[17]. This model appears more physiological than that commonly used in the

literature[18] as evidenced by a panel of Materials Science methodologies including Solid-State Nuclear Magnetic Resonance (ssNMR).

2. Materials and methods

2.1. Matrix preparation

*Collagen matrices (CollOsteoid): Type I collagen was extracted from rat tail tendons in a 0.5 M acetic acid solution and adjusted to a concentration of 3 mg/mL as previously described[19, 20]. The collagen concentration was assessed by hydroxyproline titration and the purity analyzed by SDS-PAGE. The collagen solution was progressively concentrated up to 40 mg/mL by slow evaporation of the solvent in a safety cabinet[21]. Then, 0.5 mL of the concentrated collagen solution was poured into each well of a 24 well plate and gently centrifuged at 1000 r.p.m. for 10 minutes to flatten the viscous collagen solution. Then, the fibrillogenesis was performed under ammonia vapors for 24h. Finally, matrices were rinsed with sterile PBS until neutralization of the pH.

*Mineralized collagen matrices (CollOsteoid/SBF/SBF): Mineralized collagen matrices were prepared by using the same procedure described for CollOsteoid matrices except that acidic Simulated Body Fluid (SBF) solution ($CaCl_2$ $2H_20$, NaH_2PO_4, K_2HPO_4, $NaHCO_3$, NaCl, KCl, $MgCl_2$ 6H20, Na_2 SO_4 in 0.5 M acetic acid, concentrations detailed in Table S1) was mixed with the 3 mg/mL collagen solution prior to evaporation to reach a final concentration of apatite precursors of 1.5x SBF after evaporation (Table S1) in accordance with the procedure developed by Wang *et al.*[18]. The pH was increased to induce the co-precipitation of apatite and collagen fibrils. Subsequently, matrices were immersed in 1.5x SBF[22] ($CaCl_2$ $2H_20$, NaH_2PO_4, K_2HPO_4, $NaHCO_3$, NaCl, KCl, $MgCl_2$ 6H20, Na_2 SO_4 in $(CH_2OH)_3$ CNH_2 buffer, pH = 7.4, concentrations detailed in Table S1) at 37°C for 14 days to increase the mineral content. The SBF solution was renewed each week. After 14 days, the matrices were rinsed with PBS to remove non-precipitated ions.

*Mineralized collagen matrices (CollOsteoid/CHA/SBF): Mineralized collagen matrices were prepared by using the procedure described for CollOsteoid matrices but in this work, apatite precursors salts $CaCl_2$/NaH_2PO_4/$NaHCO_3$ were dissolved into the collagen solution prior to evaporation to reach the final concentration described in the work of Nassif *et al*. [23]. As for CollOsteoid/SBF/SBF matrices, the pH increase induces the co-precipitation of carbonated hydroxyapatite (CHA) and collagen fibrils and the matrices were subsequently immersed in 1.5x SBF (pH = 7.4) at 37°C for 14 days and rinsed with PBS.

2.2. Rheological measurements

Shear oscillatory measurements on collagen matrices were performed using a Bohlin Gemini rheometer (Malvern) equipped with a plan acrylic 40 mm diameter geometry with a rough surface to prevent samples from slipping during the experiment. All tests were performed at 37°C. Mechanical spectra, namely storage, G’ and loss, G’’ moduli versus frequency, were recorded at an imposed 1% strain, which corresponds to non-destructive conditions as previously checked (Fig. S1).

2.3. Thermogravimetric analyses

Thermogravimetric analysis (TGA) was performed with a thermo-microbalance instrument (NETZSCH STA 409PC) to estimate the mineral mass of the samples. The measurements were performed from 20°C to 1000°C in an oxidizing atmosphere with a heating rate of 5°C/min.

2.4. Scanning Electron Microscopy (SEM)

Collagen matrices were fixed in 2.5% glutaraldehyde in a cacodylate solution (0.05 M). After washing in a cacodylate/saccharose buffer solution (0.05 M/0.6 M-pH 7.4), dehydration in increasing ethanol baths, matrices were dried at the carbon dioxide critical-point using a BAL-TEC 030. Samples coated with a 10 nm gold layer were observed in a Hitachi S-3400 N at an accelerating voltage of 10 kV. Energy-dispersive spectroscopy (EDS) analysis was also performed using an Oxford Instruments X-MAX detector (20 mm^2).

2.5. Transmission Electron Microscopy (TEM)

Matrices were fixed in glutaraldehyde, washed and dehydrated as described for the SEM and embedded in araldite. The matrices prepared without mineral (CollOsteoid) were additionaly post-fixed with 2% osmium tetroxyde for 1 h at 4°C prior to dehydration. Ultrathin sections (80 nm) were obtained from each kind of matrix, stained with uranyl acetate and observed in a FEI TECMAI G2 Spirit Twin electron microscope operating at 120 kV. Ultrathin sections were also observed without uranyl staining to prevent artifacts that could be assigned to the mineral particles[18].

2.6. Nuclear Magnetic Resonance

Solid state nuclear magnetic resonance (ssNMR) experiments were performed to determine the nature of the deposited mineral phase. The hydrated samples were placed in 4 mm zirconia rotors between two Teflon spacers. Magic Angle Spinning (MAS) NMR experiments at a MAS frequency of 8 kHz were performed on an AVANCE 300 Bruker spectrometer operating at $\nu(^1H)$ = 300.13 MHz and $\nu(^{31}P)$ = 121.50 MHz. For comparison, a fresh ewe bone sample from femoral or humeral metaphysis was also analyzed under the same conditions.

2.7. Osteoblast culture

Osteoblast culture: Primary human osteoblasts were obtained from knees of multiple donors at passage 2 (Promocell). Cells were grown in Dubelco's Modified Eagle culture Medium (DMEM, Gibco) containing 10% Fetal Bovine Serum (FBS, Gibco), 100 U/mL penicillin (Gibco), 100 µg/mL streptomycin, 0.25 µg/mL Fungizone (Gibco) and 10^{-8} M dexamethasone to sustain the osteoblastic phenotype[24]. Cells were kept at 37°C in a humidified atmosphere of 95% air and 5% CO_2 and the medium was replaced every two days. Using such culture conditions, osteoblasts proliferation is observed. At confluence, adherent osteoblasts were collected by treatment with 0.1% trypsin and 0.02% EDTA (Gibco).

Osteoblast culture onto collagen matrices: Osteoblasts were seeded at the surface of matrices at the density of 50,000 cells/cm^2, and grown in a differentiating medium that consists of the previously prepared medium supplemented with 50 µg/mL ascorbic acid (VWR) and 10 mM β-Glycerophosphate (Sigma)[25]. Cells were cultured on matrices for 28 days at 37°C in a humidified atmosphere of 95% air and 5% CO2. Matrices were collected at days 7, 14, 21 and 28 and processed for histological analysis, material characterization and gene expression studies.

2.8. Cell viability

To estimate the cell viability on mineralized collagen matrices, an Alamar Blue (Life Technologies) metabolic assay was performed at day 7, 14, 21 and 28. For this purpose, metabolic activity of osteoblasts cultured on the different collagen matrices was compared. This test is related to cell viability as viable cells metabolize resazurin (7-Hydroxy-3*H*-phenoxazin-3-one 10-oxide) blue dye to generate pink dye resofurin. First, matrices were washed with colorless phenol red-free culture medium and then incubated with 10% (v/v) Alamar Blue solution diluted within fresh medium for 3 hours. Subsequently, media were removed and diluted 1 in 2 colorless medium. Absorbance at 570 nm (oxidized resazurin) and 600 nm (reduced resazurin) was then recorded using an Ultrospec 1100 Pro spectrophotometer (Amersham Biosciences). For each sample, the percentage of dye reduction was calculated following the formula provided by the supplier. Metabolic activity measured with osteoblasts cultured on CollOsteoid samples at day 7 was used as reference and the other conditions were expressed as a percentage of CollOsteoid metabolic activity.

2.9. Histological analysis

Collagen matrices were fixed in 4% paraformaldehyde in PBS, dehydrated with increasing ethanol baths and embedded in paraffin for sectioning. Seven microns thick sections cut perpendicularly to the cell layer were deparaffinized, rehydrated and stained specifically with Hemalum (Hematoxylin acidic solution), staining the cellular nuclei or Von Kossa (VK), identifying phosphate groups. The sections were rinsed, dehydrated and mounted between slide and coverslip for observation using an optical microscope (Nikon E600 POL).

2.10. Migration quantification

For each matrix at each time, cell number counting was performed on 10 different histological thin sections and the result expressed as a mean per section at different depths.

2.11. Immunohistology: Alkaline Phosphatase (ALP), Gelatinase A (MMP-2), Dentin matrix protein (*DMP1*), *TE-7 and Sclerostin (SOST*)

The paraffin sections were first rehydrated and incubated for 6 min with a 0.2% pepsin solution (w/v) in acetic acid (10% v/v) for antigen retrieval. After washing in PBS, the sections were incubated for 30 min with 1% glycin in PBS solution (w/v). After another wash with PBS, sections were incubated for 60 min in a blocking solution (0.05% Tween-20 PBS, 1% bovine serum albumin (BSA) and 10% FBS). Different primary antibodies produced in mouse and binding specifically human ALP, Matrix Metalloproteinase 2 (MMP-2), MMP-13, BLGAP, DMP1, TE-7 and SOST (Millipore), diluted 1/100 (v/v) in a diluting solution (0.05% Tween-20 PBS and 1% BSA) were added onto the sections. Then, sections were incubated overnight at room temperature in a moist chamber. For ALP, MMP-2, MMP-13, BGLAP, TE-7 and SOST, after three PBS baths, an anti-mouse antibody labelled with rhodamine (Life Technology) was added over the section using a 1/400 (v/v) dilution. The samples were incubated for 90 min at room temperature in a dark moist chamber. After three PBS baths, slides were incubated for 15 min in a DAPI solution diluted in PBS (1/50 000 (v/v)). Finally, sections were rinsed three times in PBS, mounted and observed using a fluorescence microscope (AXIO 100 Zeiss) and imaged with a CCD camera (AxioCam MRm Zeiss). For DMP1 labelling, secondary anti-mouse IgG biotin conjugated (DAKO) was used. After three PBS baths, endogenous peroxidases were inhibited by incubation at 37 °C with 3% H_2O_2. After washing, the samples were incubated for 45 min with streptavidin/peroxydase complex (DAKO) diluted 1/300 in PBS containing NaCl (3% w/v). After three baths in PBS containing NaCl (3% w/v), Peroxydase labeling was revealed for 15 min in a dark chamber using 3-3' diaminobenzindine tetrahydrochloride (Sigma) in Tris-HCl, pH 7.6 and observed with a Nikon E600 POL microscope.

2.12. RT-PCR

Total RNA was extracted from matrices using TRIzol Reagent solution (Life Technologies). To remove remaining genomic DNA and proteins, total RNA was purified using RNeasy kit (Qiagen). RNAs were then reverse transcripted into complementary DNA (cDNA) using M-MLV RT enzyme (Life Technologies) at 37°C. PCR amplification reactions of *MMP-14, MEPE* and *SOST* were performed using appropriate selected primers (Table S2) with a thermal cycler (Mastercycler pro, Eppendorf). Cycling conditions were: initial Taq polymerase activation at 95°C for 5 min followed by 50 cycles, each cycle consisting of 30 sec denaturation at 95°C, 50 sec annealing at 59°C and 45 sec elongation at 72°C. Final elongation was performed at 72°C for 15 min. PCR products were then observed with a Gel Doc analyzer (Biorad, France) after migration in a 1% agarose gel containing 1µg/L ethidium bromide.

2.13. Measurement of gene expression

BGLAP, ALP, DMP1, fibroblast growth factor 23 (*FGF23*), *MMP-13,* collagen type I alpha 1 *(COL1A1), IBSP* and bone morphogenetic protein 2 (*BMP2*) gene expressions were quantified using real-time reverse transcriptase PCR (Q-PCR) in a Light Cycler 480 system (Roche) using the Light Cycler FastStart DNA Master plus SYBR Green I kit (Roche) at days 14, 21 and 28 with n = 3. The mRNA transcript level for each gene was normalized with the housekeeping gene GAPDH since its expression is not modified within collagen hydrogels[26]. Appropriate primers for real-time RT-PCR are listed in Table S2. Cycling conditions were: initial Taq polymerase activation at 95°C for 5 min followed by 50 cycles, each cycle consisting of 10 sec denaturation at 95°C; 15 sec annealing at 59°C and 15 sec elongation at 72°C. Then, a melting curve was obtained for each gene by increasing the temperature from 60°C to 97°C at a rate of 0.1°C/s to assess the reaction specificity. The results were analyzed using a relative quantification following the Pfaffl method[27]. For each gene, the efficiency of the target primer pairs was measured by producing a curve based on the amplification of a serial dilution of cDNA. For each target gene, a ratio was calculated by comparison with a calibration point which was the lower expressed sample and the value 1 arbitrary given to this calibration point. Results are presented as the mean relative expression ± standard deviation.

2.14. Bone histological analysis

Fresh bone samples were residual samples from a 2-year-old healthy French sheep harvested in the course of other experimentations. The sample was extracted from the metaphysis. The study was reviewed and approved by the IMM Recherche's Institutional Animal Care and Use committee (IACUC) prior to starting. The animal research center (IMM-Recherche) received an approval (n°75-14-01) on September 08th, 2008 for a period of 5 years by the “Sous-Direction de la protection Sanitaire” of the French Authorities.

Samples were fixed in 4% paraformaldehyde solution, dehydrated with increasing ethanol baths and impregnated for one week in a butyl methacrylate, methyl benzoate, polyethylene glycol and benzoyl peroxide resin solution. The polymerization was then triggered by addition of N,N-dimethyl-toluidine and the samples placed at -20°C for 48 hours. Four to eight microns thick sections were obtained using a tungsten carbide knife and the resin was removed using 2-ethoxyethylacetate, rehydrated and stained with Masson’s trichrome stain.

2.15. Statistical Analysis

Statistical significance was assessed using one-way analysis of variance (ANOVA) followed by Tukey posthoc test. The level of significance was set at a probability of $P < 0.05$ (**) or $P < 0.09$ (*). Results are expressed as mean ± standard deviation.

3. Results

3.1. Set-up and characterization of the osteoid models. Adapted from previous procedures[18, 23], mineralization of dense collagen matrices was performed by co-precipitation of apatite ion precursors and collagen. The mineral content of the resulting hybrid collagen/apatite biomimetic model was further increased by immersion of the matrices in SBF to reach a mineral to organic ratio of 14.7 ± 7.6 % w/w and 20.2 ± 2.9 % w/w for CollOsteoid/SBF/SBF and CollOsteoid/CHA/SBF, respectively (determined by TGA). These two matrices differ by their initial amount of ionic precursors which is much higher in CollOsteoid/CHA/SBF than that in CollOsteoid/SBF/SBF. Thus, the final amount of mineral tends to be slightly higher in CollOsteoid/CHA/SBF than in CollOsteoid/SBF/SBF. For both, the mineral content is relatively low compared to that of bone (66 % w/w)[28].
The deviations from the original co-precipitation procedure[18], *i.e.* PBS/culture medium *vs.* water, evaporation *vs.* injection and/or the looser collagen network, could lead to the precipitation of other phases than HA. Hence, to identify the nature of the mineral phase, ^{31}P ssNMR was performed on the matrices. This technique was chosen here since it allows the characterization of the samples over the heterogeneous bulk material in its native hydrated state. ^{31}P ssNMR spectra recorded for the mineralized matrices exhibit the typical 3.2 ppm chemical shift and the dissymmetric line shape characteristic of poorly-crystalline hydroxyapatite similar to that of fresh bone sample (*i.e.* an amorphous calcium phosphate-like layer around an apatitic core) (Fig. 1a, Fig. S2)[17, 18, 29]. These results confirm the presence of biomimetic hydroxyapatite in both CollOsteoid/SBF/SBF and CollOsteoid/CHA/SBF matrices and the absence of other calcium phosphate phases such as ACP, OCP or brushite as shown previously[17, 23].

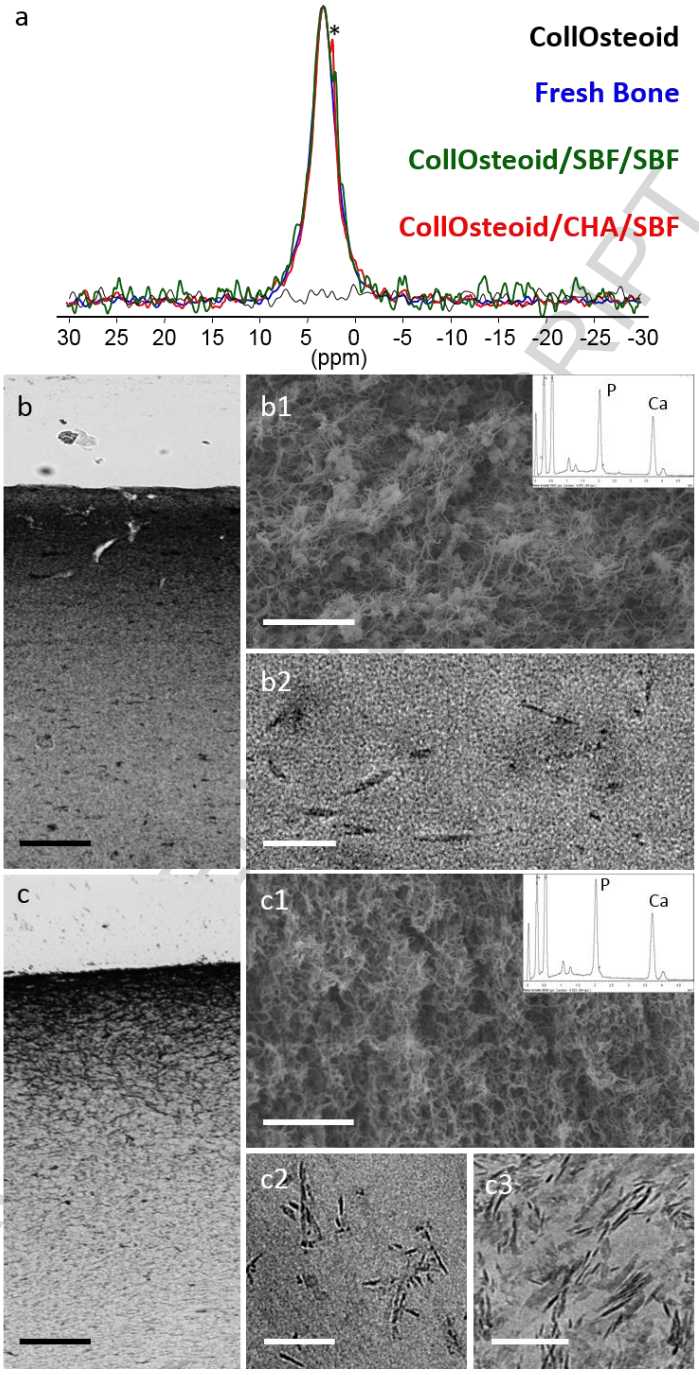

Fig. 1. Characterization of the mineral nature and distribution in dense collagen matrices. (a) ^{31}P MAS ssNMR spectra of CollOsteoid (black), CollOsteoid/SBF/SBF (green) and CollOsteoid/CHA/SBF (red) matrices and fresh bone sample (blue) exhibit the same signal at 3.2 ppm characteristic of the phosphate groups of bone apatite. The * symbol indicates phosphate buffer traces. Von Kossa staining of (b) CollOsteoid/SBF/SBF and (c) CollOsteoid/CHA/SBF (scale bar 50 µm) indicates a higher mineral deposition at the surface of the matrices. SEM observations of (b1) CollOsteoid/SBF/SBF and (c1) CollOsteoid/CHA/SBF matrices (scale bar 5 µm) show that fibrillogenesis was successfully induced and reveal the presence of HA spherulites. Inset: EDS showing the calcium and phosphate content within the mineralized matrices. TEM observations of ultrathin sections of (b2) CollOsteoid/SBF/SBF, (c2) CollOsteoid/CHA/SBF reveal intrafibrillar mineralization in c2 as it is found in (c3) mature bone (scale bar 100 nm).

The dispersion of the biomimetic hydroxyapatite and the fibrillar collagen network were studied using optical microscopy, SEM and TEM. Von Kossa's (VK) staining on histological sections allows the identification of phosphate groups. Although it is not specific to the mineral, this method is helpful to evaluate the ion dispersion within the matrices. Positive staining was observed for both mineralized matrices but appears stronger for CollOsteoid/CHA/SBF (Fig. 1b, c). Both types of mineralized matrices exhibit an ion gradient with a stronger staining on the matrix surface. To control that the staining does not result from the buffer/culture medium, VK staining was also performed on CollOsteoid matrix after 28 days of culture (Fig. S3a). Indeed, the cell culture medium is composed of apatite precursors (including Ca and P). The negative staining of CollOsteoid confirmes that the gradient is only due to the apatite mineral. As previously shown[14], the fibrillar network in CollOsteoid is dense and the fibril diameter appears quite monodisperse (Fig. S3b). Spherulites were observed in both mineralized samples (Fig. 1b1, c1). The presence of such apatite aggregates is consistent with previous observations[18] showing that the density of the collagen fibrillar network and the associated confinement have an impact on the mineral formation. Indeed, the micrometric interfibrillar spaces of the osteoid-like collagen matrix favor homogeneous extrafibrillar nucleation that leads to aggregates *vs.* isolated platelets. It can be noted that the resulting spherulites reminds of nodules formed *in vitro* from different type of bone cells*[30]*. In agreement with von Kossa's observations, SEM shows that the spherulitic crystals are more abundant on the surface of the matrices where they locally aggregate themselves (Fig. S4a and b). They appear homogeneously dispersed on the matrix surface and quite monodisperse in size (500 nm) in CollOsteoid/SBF/SBF. In contrast, they display aggregates of variable size (Fig. S4b) and are observed only locally in CollOsteoid/CHA/SBF. To complete the ssNMR study that identified the mineral phase over the whole bulk, Energy Dispersive Spectrometry (EDS) was performed to determine locally the elemental composition of the mineral. EDS analysis on CollOsteoid/SBF/SBF and CollOsteoid/CHA/SBF matrices confirm that the precipitates are mainly composed of calcium and phosphate (Fig. 1b1, 1c1, insets). The absence of signal in CollOsteoid matrix suggests the absence of non-specific precipitation (from the culture medium) in the collagen matrix (Fig. S3b, inset).

TEM observations were performed to better characterize the ultrastructure of matrices. Indeed, ionic force can modify the collagen fibrils size[31] and thus the matrix nanotopography which is described to strongly influence the cell behavior[4, 11]. To avoid any visual artifact, TEM samples were prepared with or without uranyl staining as described earlier[18]. Observations performed on stained sections distinctly show the typical cross-striated pattern of fibrils which evidences that fibrillogenesis was properly induced *in vitro* for all samples (Fig. S5a, b and c). While it is difficult to observe collagen fibrils in CollOsteoid without staining (Fig. S5d), they are observed in both mineralized matrices suggesting the presence of apatite ion precursors inside the fibrils (Fig. 1b2, c2). This is confirmed by the intrafibrillar mineralization that is locally observed in CollOsteoid/CHA/SBF. This was previously shown for denser collagen matrices[18]. Locally, apatite platelets co-align with the

main axis of the collagen fibrils as found in mature bone (Fig. 1c3). Finally, we note that the fibrils size appears to be similar for all samples but they are smaller without uranyl (~100 nm *vs*. ~60 nm in diameter, respectively) (Fig. S5).

3.2. Cell behavior on the osteoid-like models. Osteoblast viability was assessed by Alamar Blue metabolic assay. As shown in Fig. S6, osteoblast metabolic activity measured in all matrices was comparable and constant over the time course of the experiment. This observation evidences the absence of cell proliferation and is consistent with the use of differentiating medium. There are no significant differences in metabolic activity measured for the three kinds of collagen matrices suggesting a similar osteoblast adhesion onto the matrices surface.

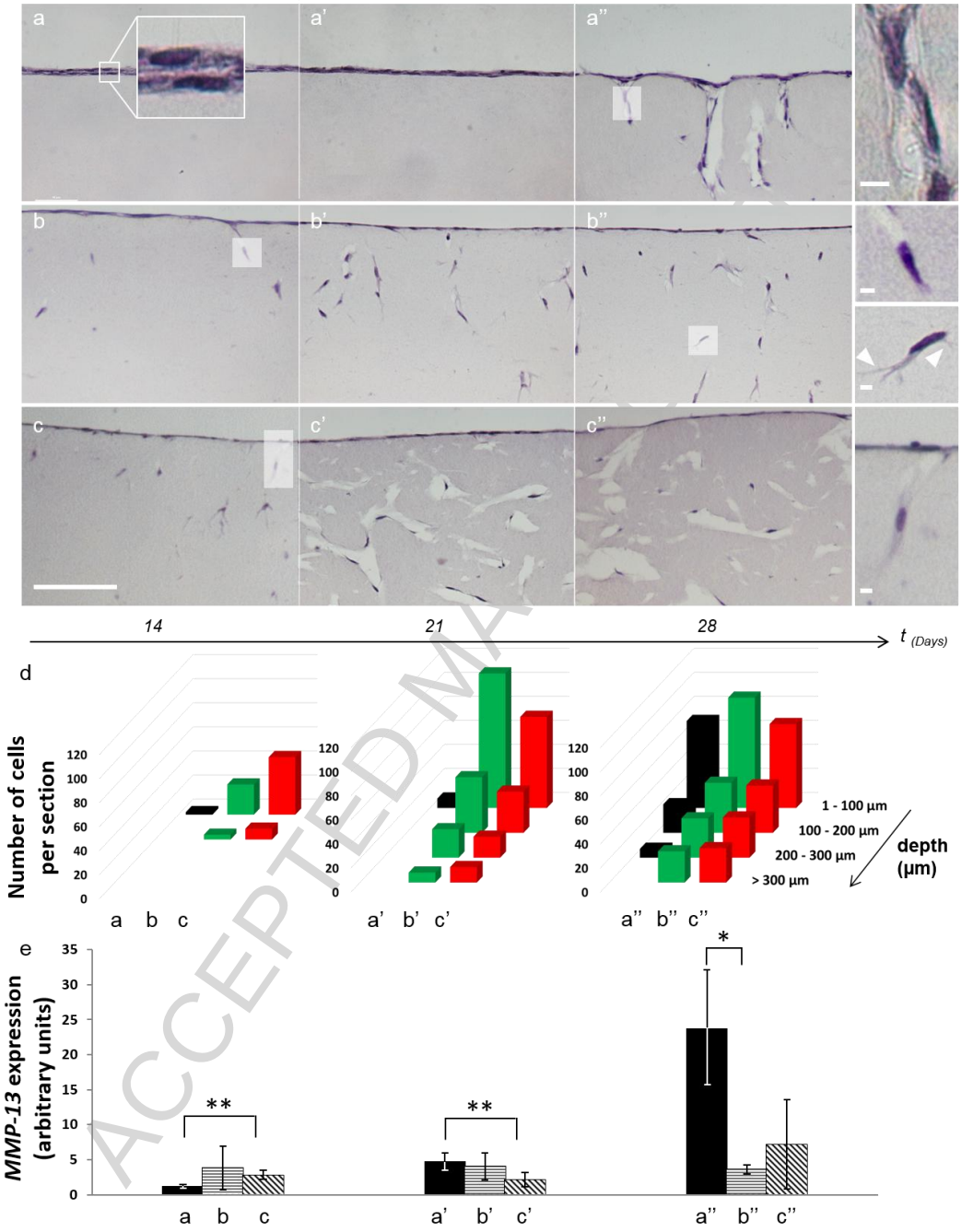

Fig. 2. Behavior of osteoblasts in osteoid-like models. Hemalum staining of (a, a' and a'') CollOsteoid, (b, b' and b'') CollOsteoid/SBF/SBF and (c, c' and c'') CollOsteoid/CHA/SBF matrices at day 14, 21 and 28, respectively, evidence the early osteoblast infiltration into the mineralized matrices. Scale bar is 100 µm. Insets are higher magnifications of entrapped cells. Arrows show cell pseudopodia. Inset scale bar is 3 µm. (d) Migration distance of osteoblasts in (a, a' and a'') CollOsteoid, (b, b' and b'') CollOsteoid/SBF/SBF and (c, c' and c'') CollOsteoid/CHA/SBF matrices at day 14, 21 and 28 of culture, respectively, expressed as number of cells per histological thin section. Standard deviations are provided in Table S3. (e) Measurement of *MMP-13* expression in (a, a' and a'') CollOsteoid, (b, b' and b'') CollOsteoid/SBF/SBF and (c, c' and c'') CollOsteoid/CHA/SBF matrices at day 14, 21 and 28, respectively, show their involvement in the degradation of the collagen matrix since this gene expression is related to the number of cells observed inside the matrix. The vertical bars on each histogram represent the standard deviation.

The behavior of osteoblasts seeded onto the matrices was analyzed with histological sections stained with Hemalum over 28 days (Fig. 2). A mono-layer (vs. a double-layer in CollOsteoid) of osteoblasts is observed on the surface of the CollOsteoid/SBF/SBF and CollOsteoid/CHA/SBF mineralized matrices (Fig. 2b, c). Some cells are also found inside the matrices over about 1 to 100 µm in depth (Fig. 2c inset, d and Table S3 day 14). The number of cells inside CollOsteoid/SBF/SBF and CollOsteoid/CHA/SBF increased with time spreading over 300 µm at day 21 (Fig. 2b', c', d and Table S3 day 21). In contrast, osteoblasts remain on the CollOsteoid matrix surface (Fig. 2a'). After 28 days, osteoblasts are found inside the matrix over 200 µm forming tracks (Fig. 2a'' and inset).

Interestingly, more osteoblasts are found inside the mineralized matrices (Fig. 2d and Table S3 day 28) and they migrated further at this time point (Fig. 2b'', c'', S7). They also possess pseudopodia. The presence of such cell protrusion indicates an active sensing and motility behavior (Fig. 2b'' inset).

In all matrices, lacunae are observed around the cells located inside the matrix. They appear larger in CollOsteoid/CHA/SBF suggesting a higher level of matrix degradation (Fig. 2c'). The presence of such gaps in the vicinity of the cells may result from the histological preparation and/or the orientation of the knife cut section. To clarify this point, the relative quantification of *MMP-13* expression was performed by Q-PCR. MMP-13 is one of the major osteoblast MMPs involved in the degradation of collagen and in bone remodeling[32]. *MMP-13* expression measured in CollOsteoid at day 14 was used as a reference (Fig. 2e). It is interesting to show that *MMP-13* is consistently expressed from day 14 by osteoblasts in the mineralized matrices whereas there is a marked increase in expression over time in CollOsteoid (the expression being lower at day 14, but much higher from day 21). The presence of MMP-2 was detected by immunohistochemistry in all matrices. This enzyme is described to be involved in bone formation.

MMP-2 is not detected in all samples at day 7 (Fig. S8a, b and c). At day 28, a MMP-2 labelling is observed in osteoblasts located within and on the surface of all matrices (Fig. S8a'', b'' and c''). Finally, the expression of *MMP-14* which encodes for a membrane metalloproteinase known to activate MMP-2 and *MMP-13* was also studied using RT-PCR. This gene is consistently expressed during the experiment (Fig. S8g). From these results, a correlation between *MMP-13* expression and the presence of lacunae can be done. It is intriguing to emphasize that this degradation activity may thus be correlated to the migration of osteoblasts. To exclude the possible dedifferentiation (*e.g.* into fibroblasts), the cell phenotype was studied.

3.3. Phenotype of osteoblasts cultured on osteoid-like models.

Alkaline Phosphatase (ALP) is a well-known osteoblastic marker involved in the mineralization process[33]. ALP was detected at the protein level by immunohistochemistry (Fig. 3a'', b'', c''). At day 28, a strong ALP labelling is detected in osteoblasts cultured in all samples regardless of their location (lining or cells inside the matrix). *ALP* expression is known to be weak in osteocytes[3]. Accordingly, we compared the different levels of *ALP*

expression in all matrices over time using Q-PCR (Fig. 3d). *ALP* expression measured in CollOsteoid matrices gradually decreases. In contrast, the expression in the mineralized matrices increases at day 21 for CollOsteoid/SBF/SBF while it remains stable for CollOsteoid/CHA/SBF. However, *ALP* expression is higher in mineralized matrices than that measured in CollOsteoid from day 21.

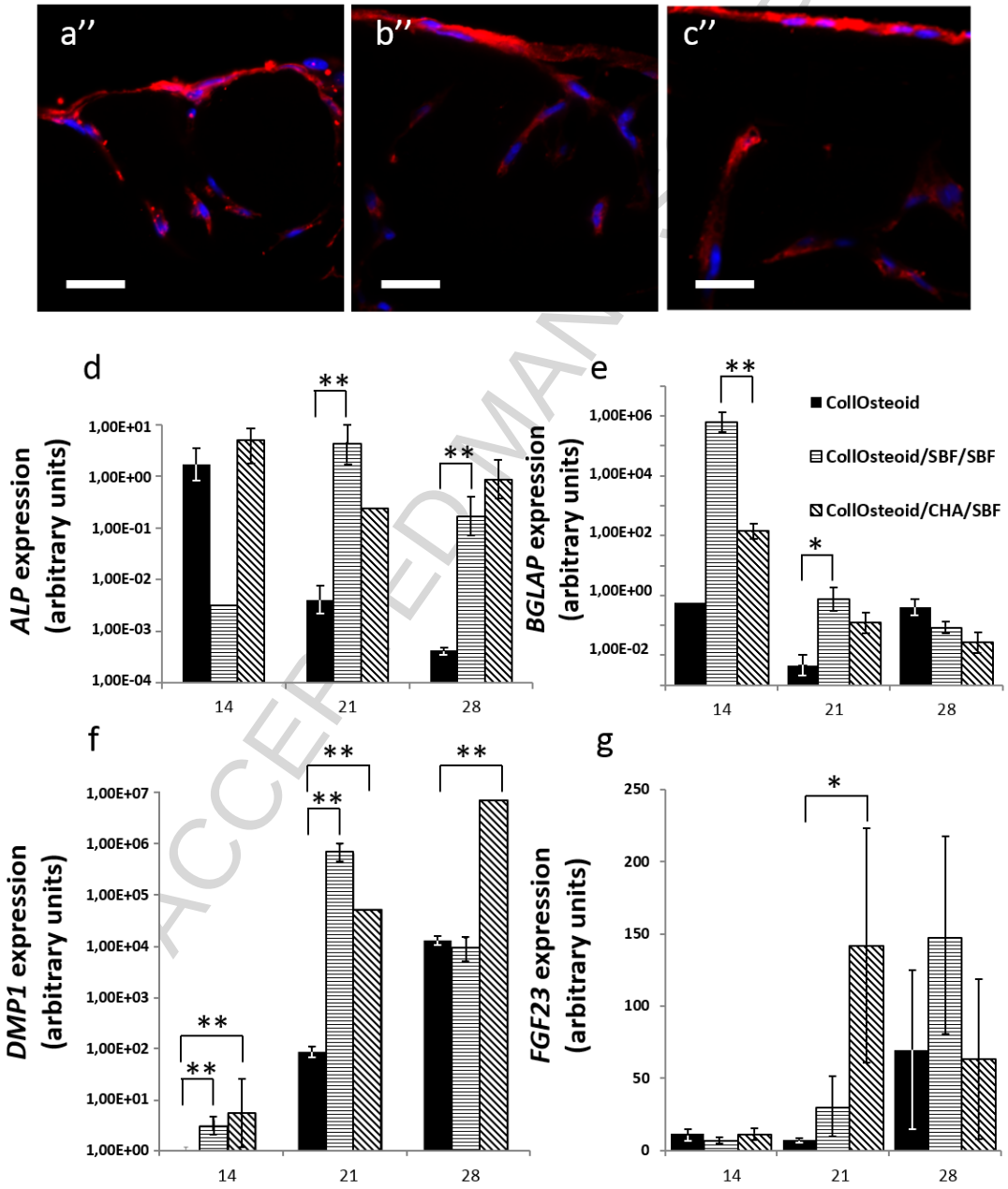

Fig. 3. Osteoblast phenotype. ALP immunodetection in (a'') CollOsteoid (b'') CollOsteoid/SBF/SBF (c'') CollOsteoid/CHA/SBF matrices at day 28 (nuclei and ALP are shown in blue and red, respectively). Scale bar is 50 µm. Quantitative real-time RT-PCR of osteoblastic markers: (d) *ALP* and (e) *BGLAP* and osteocytic differentiation markers: (f) *DMP1* and (g) *FGF23*.

Additionally, the expression of osteoblastic marker *BGLAP* (encoding for osteocalcin) was also measured (Fig. 3e). *BGLAP* expression is relatively constant in CollOsteoid. Interestingly, in the mineralized matrices, *BGLAP* is highly expressed at day 14 (about 100 times for CollOsteoid/SBF/SBF and one million times for CollOsteoid/CHA/SBF higher than in CollOsteoid) but tends to decrease to reach the expression found for CollOsteoid at 28 days.

The changes in gene expression of osteoblast toward an osteocytic phenotype include an upregulation of both the dentin matrix protein 1 (*DMP1*) and the fibroblast growth factor 23 (*FGF23*). At each time point of the study, the expression of *DMP1* is higher in the mineralized matrices than in CollOsteoid (Fig. 3f). Interestingly, the expression increases in CollOsteoid at day 14 to reach its maximum at day 28 while the highest expression is reached earlier (at day 21) for the mineralized matrices. Moreover, between day 14 and day 21, the expression of *DMP1* increases by 4 *vs.* 3 orders of magnitude with and without mineral, respectively. The presence of DMP1 was also verified at the protein level by immunochemistry (Fig. S9).

For *FGF23*, the expression is constant in CollOsteoid until day 21 (Fig. 3g). At day 28, it dramatically increases (50 times) reaching the expression found for the mineralized matrices. In the presence of mineral, the expression increases from day 14 to reach its maximum at days 21 and 28 for CollOsteoid/CHA/SBF and CollOsteoid/SBF/SBF, respectively.

To complement the phenotype study, the expression of *MEPE*, a NCP involved in the differentiation of osteoblasts into osteocytes[34, 35] was investigated by final point RT-PCR (Fig. S10). *MEPE* is expressed by the osteoblasts all over the study and appears not to be related to the presence of apatite.

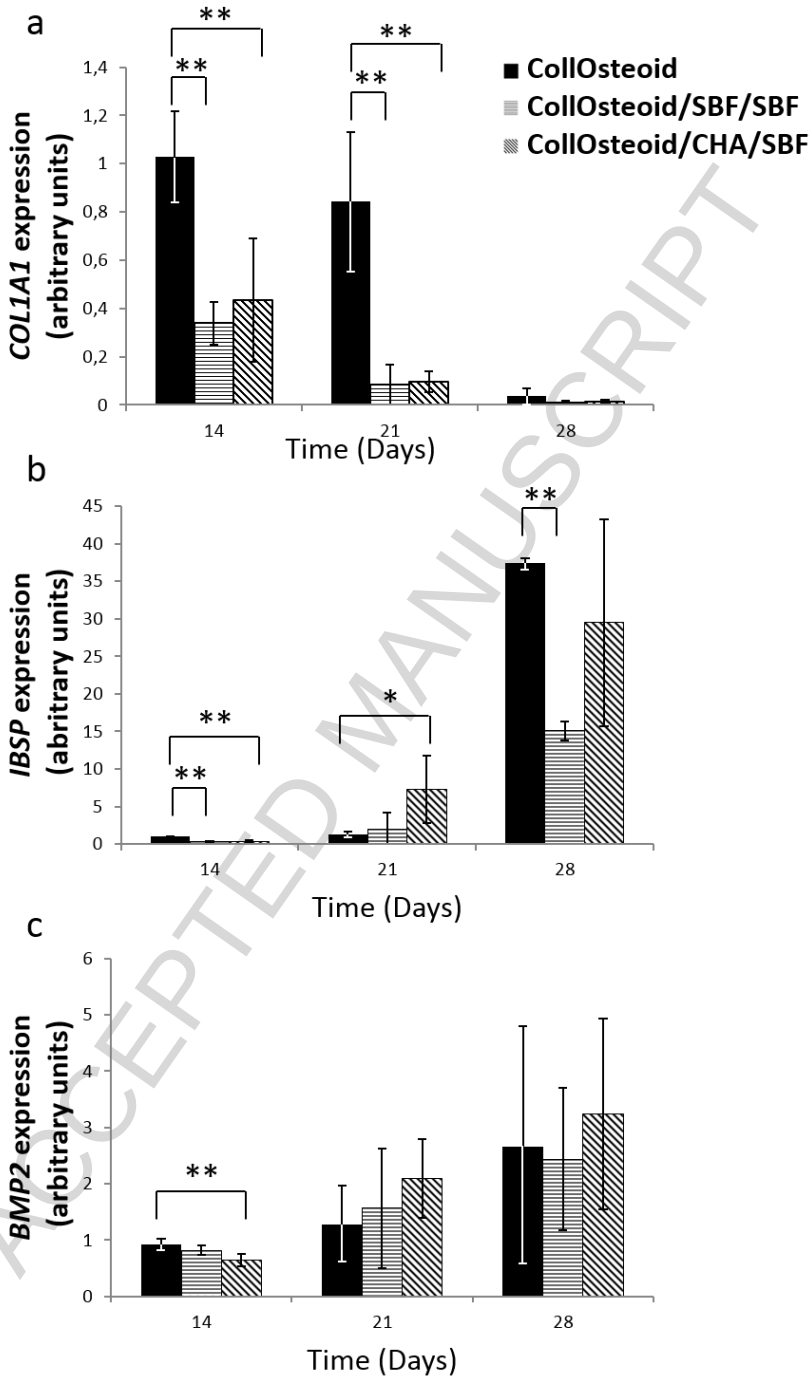

Fig. 4. Quantitative real-time RT-PCR of osteoblastic phenotype indicators. (a) *COL1A1*, (b) a mineralization gene *IBSP* and (c) bone morphogenic gene *BMP-2***.**

Taking into account that the osteocyte ECM protein production level is lower than that of the osteoblasts[3], the expression of collagen by osteoblasts was used as an indicator of their differentiation into osteocytes. Expression of Type I collagen gene (*COL1A1*) decreases over time in all matrices (Fig. 4a).The expression is lower in the mineralized matrices than in CollOsteoid until day 28; then, it is not detected in all matrices.

IBSP is a gene that encodes for one of the main bone proteins involved in the mineralization process and bone cell differentiation[36]. It is barely detected at day 14 (Fig 4b). Then, the gene expression increases during the study in all matrices but starts earlier in CollOsteoid /CHA/SBF. This result suggests that the migration and/or the presence of biomimetic hydroxyapatite orients osteoblasts toward a mineralization phenotype. This is further confirmed by the strong increase of *IBSP* expression at day 28 in CollOsteoid when cells start to migrate.
Finally, *BMP-2* expression slightly increased whatever the degree of mineralization (Fig. 4c) and appears to follow the slight increase in cell viability, indicating that the mineralization does not influence the secretion of this cytokine involved in the bone regeneration.

To conclude on the cell phenotype, the main osteoblastic markers, *i.e. ALP*, *MMP-13* and *BGLAP*, are expressed in all samples. It was shown that fibrillar collagen can trigger the expression of *ALP* and *BGLAP*[11]. *ALP* gene expression is sustained in mineralized matrices whereas in collagen matrices it was downregulated. In addition, negative TE-7 immunolabelling shows that cells did not differentiate into fibroblasts. Thus, cells found at the surface of matrices are still osteoblasts.
BGLAP gene expression in mineralized matrices is downregulated over the time although this expression is higher than that in pure collagen matrices until day 21. Moreover, *COL1A1* expression decreases and is downregulated earlier in mineralized matrices. The downregulation of *BGLAP* in late osteoblasts and the inhibition of collagen synthesis are two characteristics of the osteocyte differentiation[37]. The upregulation of *DMP1* and *FGF23* confirms that a fraction of cells started the transition toward the osteocyte phenotype. These markers evidence the presence of osteoid osteocytes or mineralizing osteocytes[2]. This is confirmed by the downregulation of *BGLAP* despite the fact that this marker is still expressed.
It is interesting to notice that *SOST*, a specific marker of mature osteocytes, is not detected during the study neither at the gene nor at the protein level. The presence of osteoblasts embedded within the mineralized matrix cannot be excluded. However, cells do not display biosynthetic activity. Instead, they show a remodeling profile (synthesis of MMPs *vs.* ECM proteins). Finally, the presence of pseudopodia observed in Fig. 2 may be suggestive of the first formation step of the osteocytes cytoplasmic extensions[1] .
Hence, the results show that the presence of bone apatite in collagen promotes the maturation of osteoblasts into mineralizing osteocytes (referred as stage 5 in Dallas *et al.*[2]).

3.4. Physico-chemical parameters influencing the osteoblast migration. To determine the material parameters that can influence the osteoblast migration, several physico-chemical parameters were investigated. As mentioned above, the mineralization degree does not appear to be significantly different in CollOsteoid/SBF/SBF and CollOsteoid/CHA/SBF. Additionally, the global charge of the mineralized matrices surface is similar as demonstrated by zeta potential measurement in a previous study[18].

However, a main difference between the two mineralized matrices is the presence of intrafibrillar mineralization in CollOsteoid/CHA/SBF. Thus, the possibly different mechanical properties of the matrices were assessed by rheological measurements (Fig. S11). The storage modulus, G' and loss modulus, G" were measured *versus* frequency. No significant variation is recorded with this parameter in the 0.1–10 Hz range. For all matrices, G' is more than one decade higher than G" which is indicative of a predominant elastic behavior. A storage modulus of 4.463 ± 0.122 kPa is measured in CollOsteoid. The mineralization process based on the precipitation and the incubation in SBF (CollOsteoid/SBF/SBF) leads to a decrease of G' down to 2.578 ± 0.269 kPa. In contrast, CollOsteoid/CHA/SBF collagen matrices exhibit significantly ($p < 0.05$) higher elastic properties with G' measured at about 7.210 ± 1.890 kPa than that measured in CollOsteoid/SBF/SBF.

4. Discussion

In bone tissue, the way osteoblasts differentiate into osteocytes follows a stepwise process that correlates to their position in the subjacent tissue (Fig. 5, steps 1 to 4). It is commonly accepted that osteoblasts or progenitor cells are recruited to ensure local bone reconstruction after the bone resorption performed by osteoclasts (step 1). Then, bordering osteoblasts become self-entrapped or are embedded by neighbor cells (step 2) and differentiate into osteocytes[3] (steps 3 to 4). Similar steps are observed *in vitro* (Fig. 2a, b, c). For example, as described for step 1 *in vivo* (Fig. 5), osteoblasts form a packed sheet on the surface of the dense collagen matrices (Fig. 2a-c"). However, in our model, the decrease of *COL1A1* expression indicates that the self-entrapment or embedding by the neighbors appears unlikely. We propose that the presence of cells inside the matrix is the result of their migration. Such property offers a third alternative pathway for osteoblasts internalization in bone tissue (Fig. 5, steps 2 to 3). Interestingly, this pathway would likely explain the tri-dimensional dispersion of osteocytes observed in bone, which is more difficult to apprehend with the entrapment or the embedding processes.

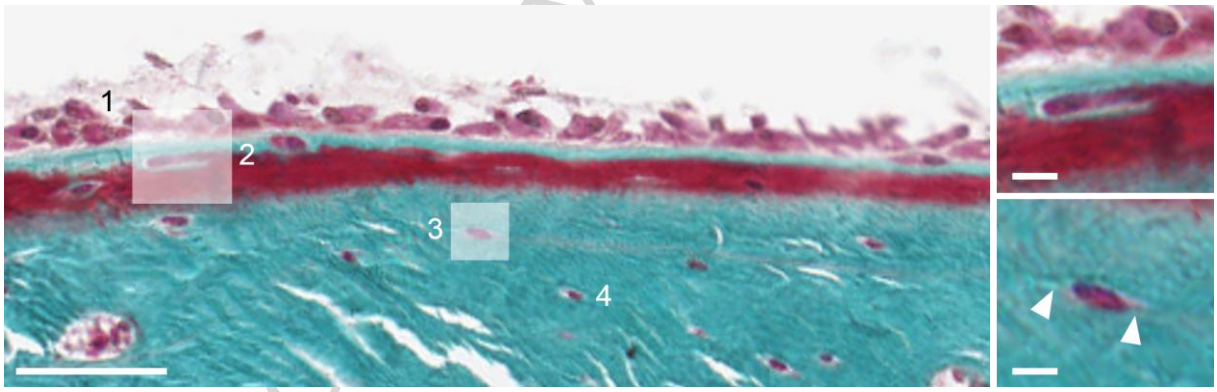

Fig. 5. Bone histological sections (Masson's trichrome) showing the osteoblast to osteocyte differentiation and illustrating the cells migration mechanism (steps 1 to 4). 1: osteoblast bordering behavior. 2: migration in osteoid collagenic ECM. 3: presence of pseudopods. 4: formation of lacunae around the cell as described for osteocytes. Scale bar 50 µm. Insets highlight cells migration. Arrows indicate the presence of pseudopods. Inset scale bar: 10 µm.

While a short-range 2D motility of pre-osteoblasts[38], dedifferentiated osteoblasts [39], osteoblasts and early osteocytes[40] over a few microns have already been reported, osteoblast and/or osteocyte 3D migration over larger distances has never been demonstrated. This can be partly explained by the fact that osteoblast-like cells or transformed cell lines that are not representative of the primary-osteoblasts [16] [41] , were used in the literature. In addition to the cellular type, we believe that the scaffolds used for the culture do not combine the essential characteristics of the osteoid tissue (*e.g.* density, structure and hydration) to favor cell migration. To the best of our knowledge, only one study reports on the migration of primary osteoblasts in a bulk scaffold made of type I collagen[42]. This hydrogel fabricated from a low concentration of collagen (3 mg/mL) exhibits

large interfibrillar spaces and is easily degraded by proteases. Hence, cell mobility is facilitated. It should also be noted that mouse (*vs.* human) osteoblasts are used in their study preventing to draw conclusions about the cell behavior in a physiological context such as the osteoid tissue.

The mechanical properties measured in pure dense collagen matrices (15 kPa) are close to those reported for the osteoid tissue (about 25 kPa [4, 12]) favoring a more physiological behavior of osteoblasts in our models than in looser gels[4]. The initial number of seeded cells also appears of great importance since a lower initial number of cells may slow down the migration process[13].

In contrast to *COL1A1*, Matrix Metalloproteinases (MMPs) are highly expressed (Fig. 2e). The expression of *MMP-13* increases over the course of the experiment. Furthermore, *MMP-14* expression is detected at each time point whereas MMP-2 is only detected at day 28 (Fig. S8). Hence, this suggests that osteoblast migration mainly relies on the matrix degradation as described for other types of cells[43, 44]. It is worth mentioning that it is only observed in the pure collagen matrix when *MMP-13* is maximal (Fig. 2). Moreover, it starts earlier in the presence of mineral (14 days *vs.* 28) which appears concomitant with the presence of cells inside the matrices. Hence, this pathway would imply a more "active" behavior of osteoblasts than those described in the literature, *i.e.* self-entrapment or embedding processes. The interfibrillar spaces in dense collagen matrices being much smaller than the cell size, osteoblasts need to digest the matrix to move. It is interesting to note that MMP activities were also detectable for primary pre-osteoblasts encapsulated in dense collagen scaffolds obtained by plastic compression although cell migration was not detected[12]. Our results confirm the ability of osteoblasts to digest the ECM in an appropriate environment as reproduced here in the osteoid models. The constant viability of osteoblasts through the experiment suggests that the differentiated phenotype of osteoblasts is favored in all matrices. This finding is further strengthened by the constant expression of *BMP-2* (Fig. 4).

A short term cytotoxicity was described earlier for apatite nanocrystals on MC3T3 type osteoblasts[45]. Here, the presence of mineral does not have any impact on the cell adhesion and viability. The use of biomimetic carbonated apatite *vs*. more crystalline hydroxyapatite possibly explain this difference in behavior. We can notice that the influence of the degree of mineralization on 2D pre-osteoblasts migration was previously discussed[38] , and shown here in 3D with osteoblasts.

Questions arise about the identification of the main parameters involved in the osteoblast migration to ensure that this pathway can indeed occur *in vivo*. The matrix stiffness is described to be involved in bone remodeling by up-regulating *MMP-13* expression level in a transient way[46]. Because *MMP-13* expression and the osteoblast migration are similar in both mineralized matrices that possess different stiffness (2.600 kPa *vs*. 7.200 kPa for CollOsteoid/SBF/SBF and CollOsteoid/CHA/SBF respectively, Fig. S11), the matrix stiffness should not be determinant for the expression of this collagenase and the related motility. This difference in stiffness appears consistent with the presence of bigger size of mineral aggregates in CollOsteoid/SBF/SBF as described for other particles[47]. Finally, although local

biomimetic apatite/collagen co-alignment is observed in CollOsteoid/CHA/SBF, the stiffness is comparable to that of CollOsteoid thus confirming that this factor does not directly drive the migration, at least, in our model.

To assess the effect of nanotopography on cell migration, the question of the surface charge is of interest as the negatively charged cell membrane preferentially bonds to positively charged surfaces[48]. Nevertheless, although the zeta potential slightly increases with the mineralization (-5.4 (±0.54) mV and -6 (±0.81) mV for CollOsteoid/SBF/SBF and CollOsteoid/CHA/SBF respectively, *vs*. -12.2 (±0.7) mV for pure collagen, they remain in the same range and negative[18]. The collagen fibril diameter is also constant in all matrices and can therefore be excluded here for the discussion. Here, the slight difference in depth of migration (Δ = 50 µm) between the mineralized matrices may be attributed either to the difference in mineralization degree and/or to the presence of intrafibrillar mineralization in CollOsteoid/CHA/SBF.

The difference in apatite deposition and the large deposits at the surface with irregular spacing and shape (Fig. 1) does not alter the behavior of cells. This is consistent with previous works in the literature showing that collagen mainly directs osteoblast behavior[49]. Nevertheless, the difference in roughness due to biomimetic apatite can also affect the osteoblast migration. As shown previously, the amorphous calcium phosphate-like layer that coats the biomimetic apatite core can act as a disordered and highly soluble ion reservoir[17]. Moreover, a high local release of ions, especially calcium, is described to modify genes expression such as *ALP* [50-52]. Hence, it is likely that the structure and chemical composition of the biomimetic apatite influence various osteoblast gene expression. This hypothesis is further strengthened by observation in the literature showing that osteoblasts mediate bone apatite formation in the form of spherulitic aggregates[53].

Aside from the putative effect of apatite-derived ions on genes that is related to the osteoblast migration, genes involved in the osteoblast differentiation are modified in our model. The process of differentiation of osteocytes is largely unknown but osteoblasts are known to initiate their differentiation as soon as they are surrounded by mineralized matrices (steps 3 to 4). Notably, the expression of markers such as *BGLAP, DMP1, FGF23* and *COL1A1* is modified during the study. The modifications in gene expression are correlated to the migration and show the differentiation of cells into osteoid osteocytes or mineralizing osteocytes[2]. This differentiation is faster when bone apatite is present in the matrix (Fig. 3). This is in agreement with results in the literature showing that the mineralization of ECM is an essential regulator of osteocytogenesis[54, 55].

Overall, these results suggest that migration may be required to trigger osteocyte differentiation. Same conclusions are drawn with low collagen concentration and without mineral [42]. Concerning *IBSP*, its expression is observed almost simultaneously with the cell migration in collagen matrices regardless of the degree of mineralization (Fig. 4). Hence the presence of bone apatite promotes the expression of genes involved in the mineralization process *i.e.* IBSP and *DMP1*. These gene expressions strengthen the conclusion that a mineralization process which leads to the mineralizing osteocyte stage of differentiation is

initiated by the osteoblasts. Finally, SOST is not detected in cells. This observation may be explained by the fact that the final step of osteocyte differentiation, characterized by an inhibition of mineralization, is still not reached at the end of the study[2]. Moreover, we cannot exclude that there might still be osteoblasts embedded within the mineralized collagen matrix.

5. Conclusion

This study highlights an alternative pathway by which osteoblasts migrate from a surface to a trapped position observed for osteocytes. We demonstrate that the presence of bone apatite promotes osteoblast migration, possibly through an ions release and/or mediated by the roughness of the apatite. When compared to native bone osteoblast-to-osteocyte differentiation, our mineralized models successfully reproduce the first steps of this process up to the “osteoid osteocytes” or “mineralizing osteocytes” stages of differentiation.
Improvement of the model will include other physiological factors such as mechanical stress and extracellular flux. In addition, further studies will settle the importance of using biomimetic carbonated apatite particles (*i.e.* amorphous layer around an apatite crystalline core, platelet shape and nanometric size) compared to highly crystalized ceramics materials to induce cell colonization.

Acknowledgements
We thank Luc Behr and IMM for providing ewe bone samples, Özlem Sel and Anthony Sloan for correcting of the manuscript and Graciela Pavon-Djavid for her help in bone histological preparation. We thank the reviewers for helping to improve the science in this manuscript, in particular by pointing out key works to clarify the cells phenotype.

Author contributions

M.R., C.A., T.A., N.N. and C.H. performed the research; B.H., C.I., and J.L. performed samples preparation for microscopies and immuno-imaging; M.R., C.A., T.A., N.N., M-M.G-G. and C.H analyzed data; M.R., N.N. and C.H wrote the paper; T.A., M-M.G-G. corrected the paper; N.N. and C.H. designed the research.

References

[1] Dallas SL, Bonewald LF. Dynamics of the transition from osteoblast to osteocyte. Ann N Y Acad Sci 2010;1192:437-43.
[2] Dallas SL, Prideaux M, Bonewald LF. The osteocyte: an endocrine cell and more. Endocr Rev 2013;34:658-90.
[3] Franz-Odendaal TA, Hall BK, Witten PE. Buried alive: how osteoblasts become osteocytes. Dev Dyn 2006;235:176-90.
[4] Engler AJ, Sen S, Sweeney HL, Discher DE. Matrix Elasticity Directs Stem Cell Lineage Specification. Cell 2006;126:677-89.
[5] Hirao M, Hashimoto J, Yamasaki N, Ando W, Tsuboi H, Myoui A, et al. Oxygen tension is an important mediator of the transformation of osteoblasts to osteocytes. J Bone Miner Metab 2007;25:266-76.
[6] Yan Y-x, Gong Y-w, Guo Y, Lv Q, Guo C, Zhuang Y, et al. Mechanical Strain Regulates Osteoblast Proliferation through Integrin-Mediated ERK Activation. PLoS ONE 2012;7:e35709.
[7] Guo Y, Zhang C-q, Zeng Q-c, Li R-x, Liu L, Hao Q-x, et al. Mechanical strain promotes osteoblast ECM formation and improves its osteoinductive potential. Biomed Eng Online 2012;11:80.
[8] Akhouayri O, Lafage-Proust M-H, Rattner A, Laroche N, Caillot-Augusseau A, Alexandre C, et al. Effects of static or dynamic mechanical stresses on osteoblast phenotype expression in three-dimensional contractile collagen gels. J Cell Biochem 1999;76:217-30.
[9] Jokinen J, Dadu E, Nykvist P, Kaepylae J, White DJ, Ivaska J, et al. Integrin-mediated Cell Adhesion to Type I Collagen Fibrils. J Biol Chem 2004;279:31956-63.
[10] White DJ, Puranen S, Johnson MS, Heino J. The collagen receptor subfamily of the integrins. Int J Biochem Cell Biol 2004;36:1405-10.
[11] Tsai S-W, Chen C-C, Chen P-L, Hsu F-Y. Influence of topography of nanofibrils of three-dimensional collagen gel beads on the phenotype, proliferation, and maturation of osteoblasts. J Biomed Mater Res, Part A 2008;91A:985-93.
[12] Buxton PG, Bitar M, Gellynck K, Parkar M, Brown RA, Young AM, et al. Dense collagen matrix accelerates osteogenic differentiation and rescues the apoptotic response to MMP inhibition. Bone (San Diego, CA, U S) 2008;43:377-85.
[13] Silvent J, Nassif N, Helary C, Azais T, Sire J-Y, Guille MMG. Collagen osteoid-like model allows kinetic gene expression studies of non-collagenous proteins in relation with mineral development to understand bone biomineralization. PLoS One 2013;8:e57344.
[14] Giraud Guille MM, Helary C, Vigier S, Nassif N. Dense fibrillar collagen matrices for tissue repair. Soft Matter 2010;6:4963-7.
[15] Elias KL, Price RL, Webster TJ. Enhanced functions of osteoblasts on nanometer diameter carbon fibers. Biomaterials 2002;23:3279-87.
[16] Vigier S, Helary C, Fromigue O, Marie P, Giraud-Guille M-M. Collagen supramolecular and suprafibrillar organizations on osteoblasts long-term behavior: Benefits for bone healing materials. J Biomed Mater Res, Part A 2010;94A:556-67.
[17] Wang Y, Von ES, Fernandes FM, Cassaignon S, Selmane M, Laurent G, et al. Water-mediated structuring of bone apatite. Nat Mater 2013;12:1144-53.
[18] Wang Y, Azais T, Robin M, Vallee A, Catania C, Legriel P, et al. The predominant role of collagen in the nucleation, growth, structure and orientation of bone apatite. Nat Mater 2012;11:724-33.
[19] Gobeaux F, Belamie E, Mosser G, Davidson P, Panine P, Giraud-Guille MM. Cooperative Ordering of Collagen Triple Helices in the Dense State. Langmuir 2007;23:6411-7.
[20] Helary C, Foucault-Bertaud A, Godeau G, Coulomb B, Guille MMG. Fibroblast populated dense collagen matrices: cell migration, cell density and metalloproteinases expression. Biomaterials 2005;26:1533-43.
[21] Besseau L, Coulomb B, Lebreton-Decoster C, Giraud-Guille M-M. Production of ordered collagen matrices for three-dimensional cell culture. Biomaterials 2001;23:27-36.

[22] Rhee S-H, Tanaka J. Hydroxyapatite formation on cellulose cloth induced by citric acid. J Mater Sci: Mater Med 2000;11:449-52.
[23] Nassif N, Martineau F, Syzgantseva O, Gobeaux F, Willinger M, Coradin T, et al. In Vivo Inspired Conditions to Synthesize Biomimetic Hydroxyapatite. Chem Mater 2010;22:3653-63.
[24] Coelho MJ, Cabral AT, Fernandes MH. Human bone cell cultures in biocompatibility testing. Part I: Osteoblastic differentiation of serially passaged human bone marrow cells cultured in α-MEM and in DMEM. Biomaterials 2000;21:1087-94.
[25] Coelho MJ, Fernandes MH. Human bone cell cultures in biocompatibility testing. Part II: Effect of ascorbic acid, β-glycerophosphate and dexamethasone on osteoblastic differentiation. Biomaterials 2000;21:1095-102.
[26] Barber RD, Harmer DW, Coleman RA, Clark BJ. GAPDH as a housekeeping gene: Analysis of GAPDH mRNA expression in a panel of 72 human tissues. Physiol Genomics 2005;21:389-95.
[27] Pfaffl MW. A new mathematical model for relative quantification in real-time RT-PCR. Nucleic Acids Res 2001;29:e45.
[28] Glimcher MJ. Bone: nature of the calcium phosphate crystals and cellular, structural, and physical chemical mechanisms in their formation. Rev Mineral Geochem 2006;64:223-82.
[29] Wang Y, Von Euw S, Laurent G, Crevant C, Bonhomme-Coury L, Giraud-Guille M-M, et al. Impact of collagen confinement vs. ionic substitutions on the local disorder in bone and biomimetic apatites. Mater Horiz 2014;1:224-31.
[30] Gentleman E, Swain RJ, Evans ND, Boonrungsiman S, Jell G, Ball MD, et al. Comparative materials differences revealed in engineered bone as a function of cell-specific differentiation. Nat Mater 2009;8:763-70.
[31] Gobeaux F, Mosser G, Anglo A, Panine P, Davidson P, Giraud-Guille MM, et al. Fibrillogenesis in Dense Collagen Solutions: A Physicochemical Study. J Mol Biol 2008;376:1509-22.
[32] Stahle-Baeckdahl M, Sandstedt B, Bruce K, Lindahl A, Jimenez MG, Vega JA, et al. Collagenase-3 (MMP-13) is expressed during human fetal ossification and re-expressed in postnatal bone remodeling and in rheumatoid arthritis. Lab Invest 1997;76:717-28.
[33] Harris H. The human alkaline phosphatases: what we know and what we don't know. Clin Chim Acta 1990;186:133-50.
[34] Rowe PSN, De Zoysa PA, Dong R, Wang HR, White KE, Econs MJ, et al. MEPE, a new gene expressed in bone marrow and tumors causing osteomalacia. Genomics 2000;67:54-68.
[35] Hayashibara T, Hiraga T, Yi B, Nomizu M, Kumagai Y, Nishimura R, et al. A synthetic peptide fragment of human MEPE stimulates new bone formation in vitro and in vivo. J Bone Miner Res 2004;19:455-62.
[36] Ganss B, Kim RH, Sodek J. Bone sialoprotein. Crit Rev Oral Biol Med 1999;10:79-98.
[37] Boukhechba F, Balaguer T, Michiels J-F, Ackermann K, Quincey D, Bouler J-M, et al. Human primary osteocyte differentiation in a 3D culture system. J Bone Miner Res 2009;24:1927-35.
[38] Perrier A, Dumas V, Linossier MT, Fournier C, Jurdic P, Rattner A, et al. Apatite content of collagen materials dose-dependently increases pre-osteoblastic cell deposition of a cement line-like matrix. Bone (Amsterdam, Neth) 2010;47:23-33.
[39] Knopf F, Hammond C, Chekuru A, Kurth T, Hans S, Weber CW, et al. Bone Regenerates via Dedifferentiation of Osteoblasts in the Zebrafish Fin. Dev Cell 2011;20:713-24.
[40] Dallas SL, Veno PA, Rosser JL, Barragan-Adjemian C, Rowe DW, Kalajzic I, et al. Time lapse imaging techniques for comparison of mineralization dynamics in primary murine osteoblasts and the late osteoblast/early osteocyte-like cell line MLO-A5. Cells Tissues Organs 2009;189:6-11.
[41] Czekanska EM, Stoddart MJ, Ralphs JR, Richards RG, Hayes JS. A phenotypic comparison of osteoblast cell lines versus human primary osteoblasts for biomaterials testing. J Biomed Mater Res, Part A 2014;102A:2636-43.
[42] Uchihashi K, Aoki S, Matsunobu A, Toda S. Osteoblast migration into type I collagen gel and differentiation to osteocyte-like cells within a self-produced mineralized matrix: A novel system for analyzing differentiation from osteoblast to osteocyte. Bone (N Y, NY, U S) 2013;52:102-10.

[43] Ortega N, Behonick D, Stickens D, Werb Z. How proteases regulate bone morphogenesis. Ann N Y Acad Sci 2003;995:109-16.
[44] Paiva KBS, Granjeiro JM. Bone tissue remodeling and development: Focus on matrix metalloproteinase functions. Arch Biochem Biophys 2014;561:74-87.
[45] Chou Y-F, Huang W, Dunn JCY, Miller TA, Wu BM. The effect of biomimetic apatite structure on osteoblast viability, proliferation, and gene expression. Biomaterials 2005;26:285-95.
[46] D'Alonzo RC, Kowalski AJ, Denhardt DT, Nickols GA, Partridge NC. Regulation of collagenase-3 and osteocalcin gene expression by collagen and osteopontin in differentiating MC3T3-E1 cells. J Biol Chem 2002;277:24788-98.
[47] Alvarez GS, Helary C, Mebert AM, Wang X, Coradin T, Desimone MF. Antibiotic-loaded silica nanoparticle-collagen composite hydrogels with prolonged antimicrobial activity for wound infection prevention. J Mater Chem B 2014;2:4660-70.
[48] Chen L, McCrate JM, Lee JCM, Li H. The role of surface charge on the uptake and biocompatibility of hydroxyapatite nanoparticles with osteoblast cells. Nanotechnology 2011;22:105708/1-/10.
[49] Stevens MM, George JH. Exploring and engineering the cell surface interface. Science 2005;310:1135-8.
[50] Yuasa T, Miyamoto Y, Ishikawa K, Takechi M, Momota Y, Tatehara S, et al. Effects of apatite cements on proliferation and differentiation of human osteoblasts in vitro. Biomaterials 2004;25:1159-66.
[51] Maxian SH, Di Stefano T, Melican MC, Tiku ML, Zawadsky JP. Bone cell behavior on Matrigel-coated Ca/P coatings of varying crystallinities. J Biomed Mater Res 1998;40:171-9.
[52] Sugimoto T, Kanatani M, Kano J, Kaji H, Tsukamoto T, Yamaguchi T, et al. Effects of high calcium concentration on the functions and interactions of osteoblastic cells and monocytes and on the formation of osteoclast-like cells. J Bone Miner Res 1993;8:1445-52.
[53] Boonrungsiman S, Gentleman E, Carzaniga R, Evans ND, McComb DW, Porter AE, et al. The role of intracellular calcium phosphate in osteoblast-mediated bone apatite formation. Proc Natl Acad Sci U S A 2012;109:14170-5, S/1-S/6.
[54] Prideaux M, Loveridge N, Pitsillides AA, Farquharson C. Extracellular matrix mineralization promotes E11/gp38 glycoprotein expression and drives osteocytic differentiation. PLoS One 2012;7:e36786.
[55] Irie K, Ejiri S, Sakakura Y, Shibui T, Yajima T. Matrix mineralization as a trigger for osteocyte maturation. J Histochem Cytochem 2008;56:561-7.

SUPPLEMENTARY INFORMATION

Involvement of 3D osteoblast migration and bone apatite during *in vitro* early osteocytogenesis

Marc Robin[a], Claudia Almeida[a], Thierry Azaïs[a], Bernard Haye[a], Corinne Illoul[a], Julie Lesieur[b], Marie-Madeleine Giraud-Guille[a], Nadine Nassif[a,*], Christophe Hélary[a,*]

[a] *Sorbonne Universités UPMC Univ Paris 06, CNRS, Collège de France, Laboratoire Chimie de la Matière Condensée de Paris UMR 7574, 11 place Marcelin Berthelot 75005 Paris, France*

[b] *EA 2496, Pathologies, Imaging and Biotherapies of the Tooth, UFR Odontologie, University Paris Descartes PRES Sorbonne Paris Cite, Montrouge, France*

Corresponding authors: nadine.nassif@upmc.fr ; christophe.helary@upmc.fr

Table S1. Concentration of salts used for the preparation of mineralized collagen matrices

Concentration (mM)	$CaCl_2 2H_20$	NaH_2PO_4	K_2HPO_4	$NaHCO_3$	NaCl	KCl	$MgCl_2 6H_20$	$Na_2 SO_4$	$(CH_2OH)_3 CNH_2$
CHA [23]	110	33	-	33	-	-	-	-	-
1.5x SBF solution (in 0.5 M acetic acid)	3.8	-	1.5	6.3	213	4.5	2.3	0.75	-
1.5x SBF solution (pH = 7.4)	3.8	-	1.5	6.3	213	4.5	2.3	0.75	10

Table S2. Primers sequences

Target	Sequences
GAPDH	TTGATTTTGGAGGGATCTCG GAGTCAACGGATTTGGTCGT
ALP	GCAGCTTGACCTCCTCGGAAGACACT TCACCGCCCACCACCTTGTAGCC
BGLAP	ACATTTCTGTCCTCTGCGCGTGGTT CCCCAGTCCCCTACCCGGAT
IBSP	AACGAACAAGGCATAAACGGCACCA CTTGCCCTGCCTTCCGGTCT
COL1A1	CCAGTCAGAGTGGCACATCTTGA GCTCACGATGGTGCCGCTACTA
BMP2	TCATCTGAACTCCACTAATCATGCC TTTGCTGTACTAGCGACACCCA
MMP-13	GCCGGTGTAGGTGTAGATAGGAAA GGAGATGCCCATTTTGATGATGA
MMP-14	CTGGATGCAGAAAGTGATTTCATTA TCGCTGCCATGCAGAAGTTTTA
MEPE	GGGCCTGCCCATTCCTTCTCGT ACCCCAGGAGCCTTTCCCTTGTG
SOST	TCTCAATTCCCTCCCCTGCCCCGTG CCAGCAGAGCGACACCCTAGACC
DMP1	ACCAAGATGACAATGACTGCC CAAGTGTAATGTCCAGCAATTCCT
FGF23	CACCCCATCAGACCATCTACAGTGC TCTCCGGGTCGAAATAGTGTGATCCAA

Table S3. Evidence of in-depth migration of osteoblasts in osteoid-like models at days 14, 21 and 28 of culture expressed as number of cells per histological thin section.

Days	1-100 µm	100-200 µm	200-300 µm	> 300 µm
14				
CollOsteoid	2 ± 1	0	0	0
CollOsteoid/SBF/SBF	25 ± 4	4 ± 2	0	0
CollOsteoid/CHA/SBF	48 ± 14	9 ± 3	0	0
21				
CollOsteoid	8 ± 3	0	0	0
CollOsteoid/SBF/SBF	112 ± 23	46 ± 8	24 ± 7	8 ± 4
CollOsteoid/CHA/SBF	76 ± 8	34 ± 8	17 ± 3	13 ± 4
28				
CollOsteoid	72 ± 12	24 ± 6	7 ± 4	0
CollOsteoid/SBF/SBF	92 ± 12	42 ± 6	33 ± 5	26 ± 4
CollOsteoid/CHA/SBF	70 ± 9	40 ± 6	33 ± 5	28 ± 5

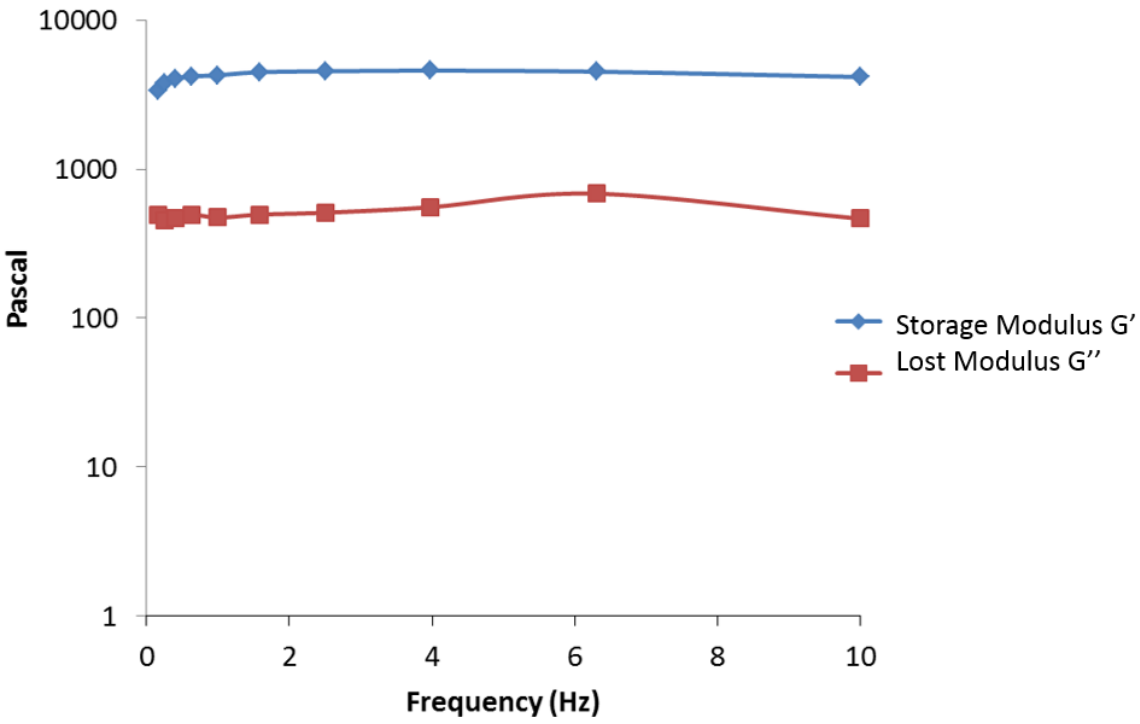

Fig. S1. Storage and lost Moduli of CollOsteoid *versus* Frequency. The conditions were not destructive as the mechanical measurements were performed at a frequency of 1Hz.

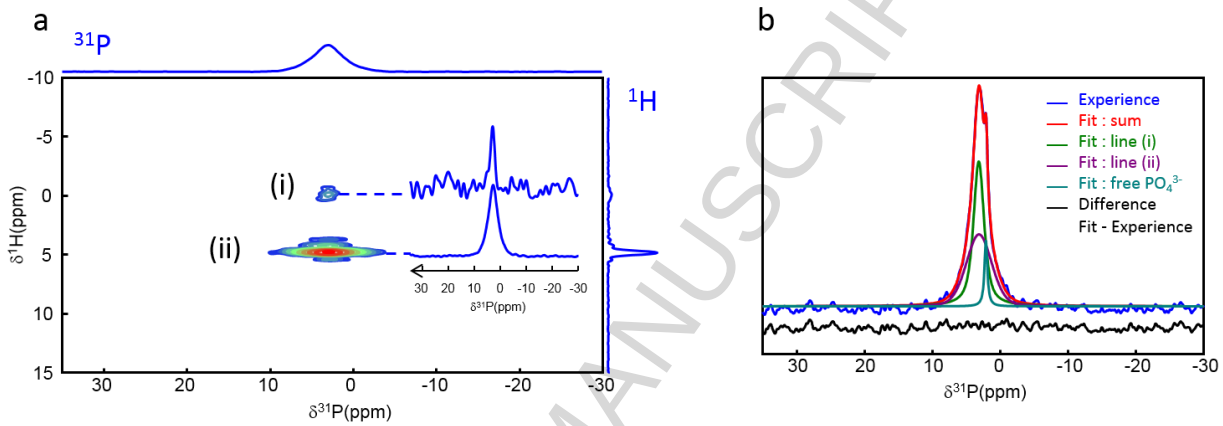

Fig. S2. Structural investigation of mineral by solid-state NMR. (a) 2D ^{1}H-^{31}P HetCor spectrum of CollOsteoid/CHA/SBF (contact time = 10 ms) display the two distinct domains composing the apatite platelets: (*i*) the apatitic core where orthophosphate ions ($\delta(^{31}P)$ = 3 ppm) correlates with OH^- (δ (^{1}H) = 0 ppm and (*ii*) the hydrated disordered layer where HPO_4^{2-} ions ($d(^{31}P)$ = 3.2 ppm) correlates with water molecules ($\delta(^{1}H)$ = 4.9 ppm). This core-layer organization was also described for bone apatite platelets[17]. (b) The 1D ^{31}P NMR spectrum of CollOsteoid/CHA/SBF (blue line) can be quantitatively fitted using the ^{31}P line shapes extracted from the previous 2D experiments: apatitic phosphates (green line; 47%), surface HPO_4^{2-} (purple line; 48%) and free phosphate from the buffer solution (5%). These proportions are consistent with data found for bone apatite platelets[17].

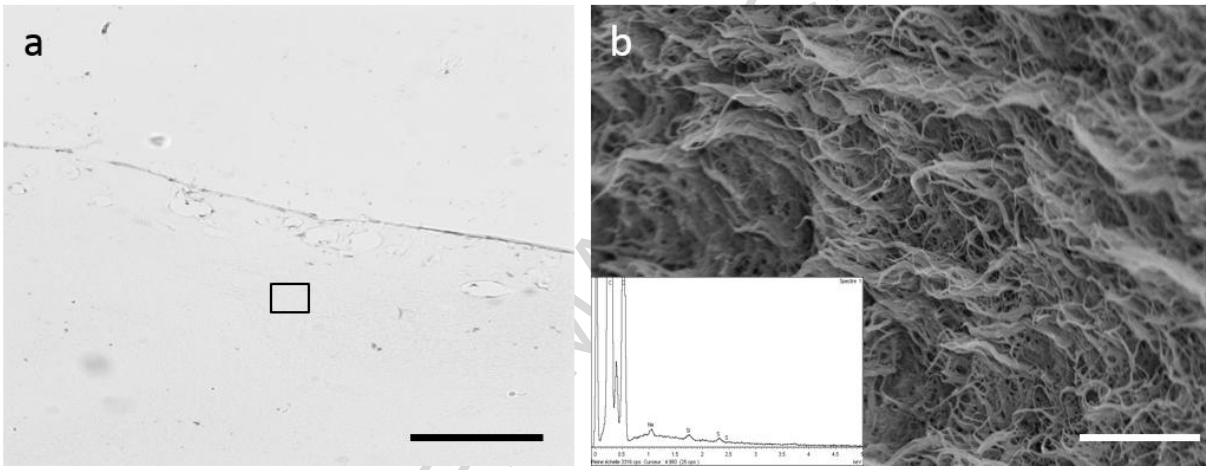

Fig. S3. CollOsteoid matrix structure. (a) Paraffin section stained with VK staining shows the absence of phosphate groups. Scale bar 100 µm. (b) SEM observation of a dense collagen matrix at 40 mg/mL. Scale bar 5 µm. Inset: EDS confirms the absence of calcium and phosphate.

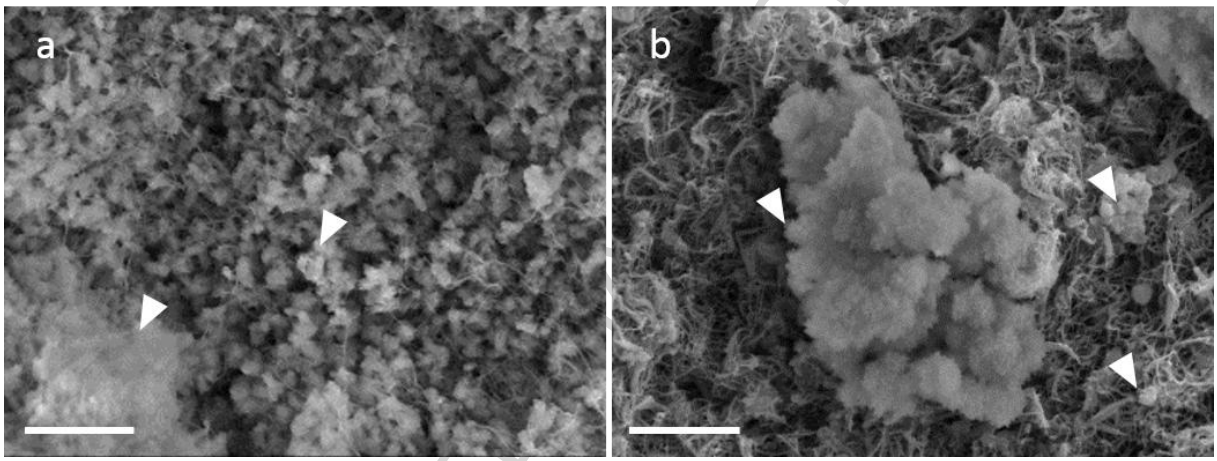

Fig. S4. SEM observations of the surface of the mineralized matrices. (a) CollOsteoid/SBF/SBF matrix mainly exhibits spherulites and bigger aggregates (arrow) (b) CollOsteoid/CHA/SBF matrix shows a variety of aggregate sizes (arrows). Scale bar 5 µm.

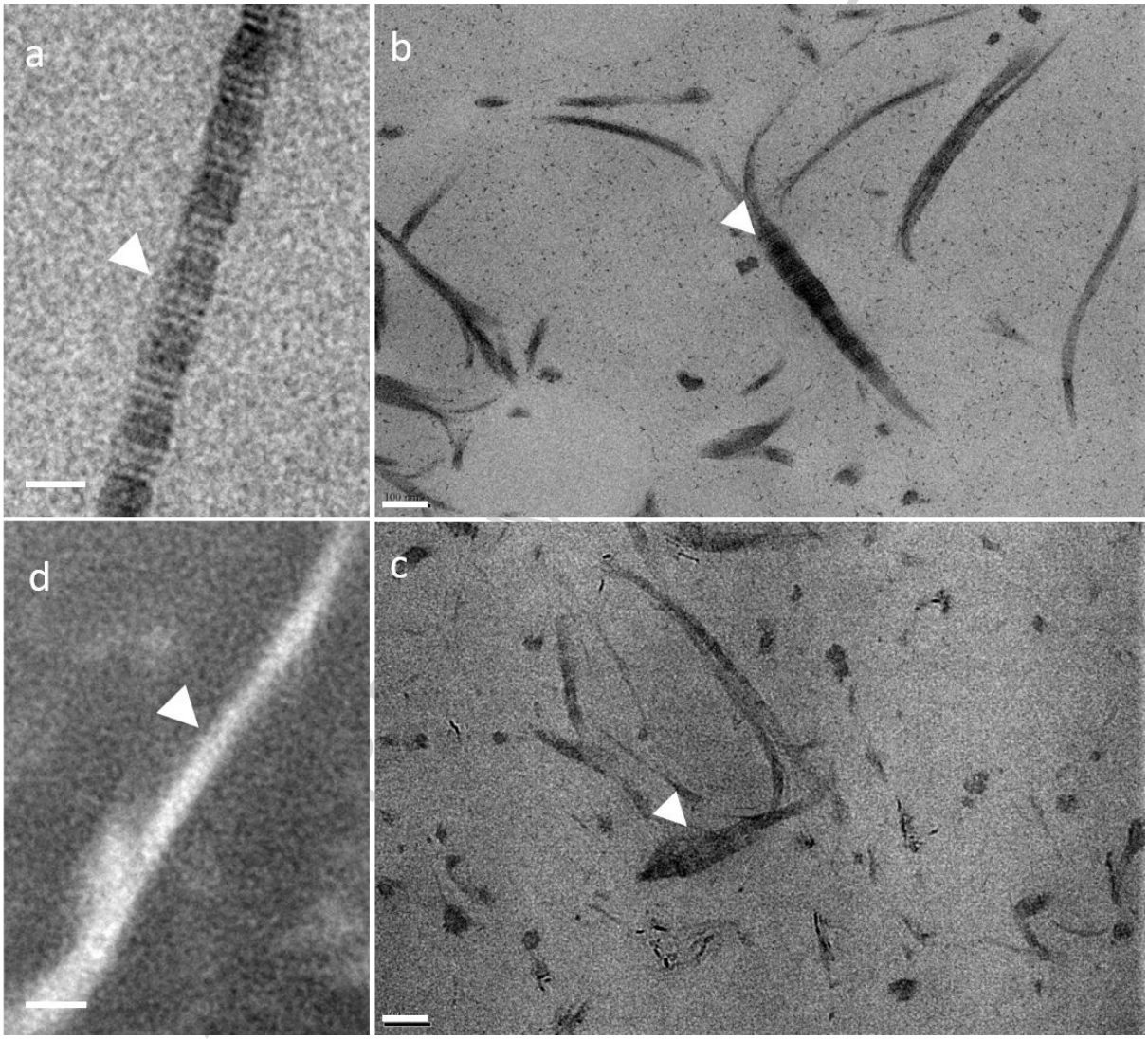

Fig. S5. Investigation of the matrices at the fibrillar level. Arrows point out collagen fibrils. TEM observations of uranyl-stained ultrathin sections of (a) CollOsteoid, (b) CollOsteoid/SBF/SBF, (c) CollOsteoid/CHA/SBF. (d) Without staining, the typical cross-striation is hardly observed in CollOsteoid. The presence of typical cross-striation in collagen fibrils evidences that the fibrillogenesis was properly induced. Visual artifacts due to the uranyl staining are observed in the background of the fibrils in (a), (b) and (c). Scale bar 100 nm.

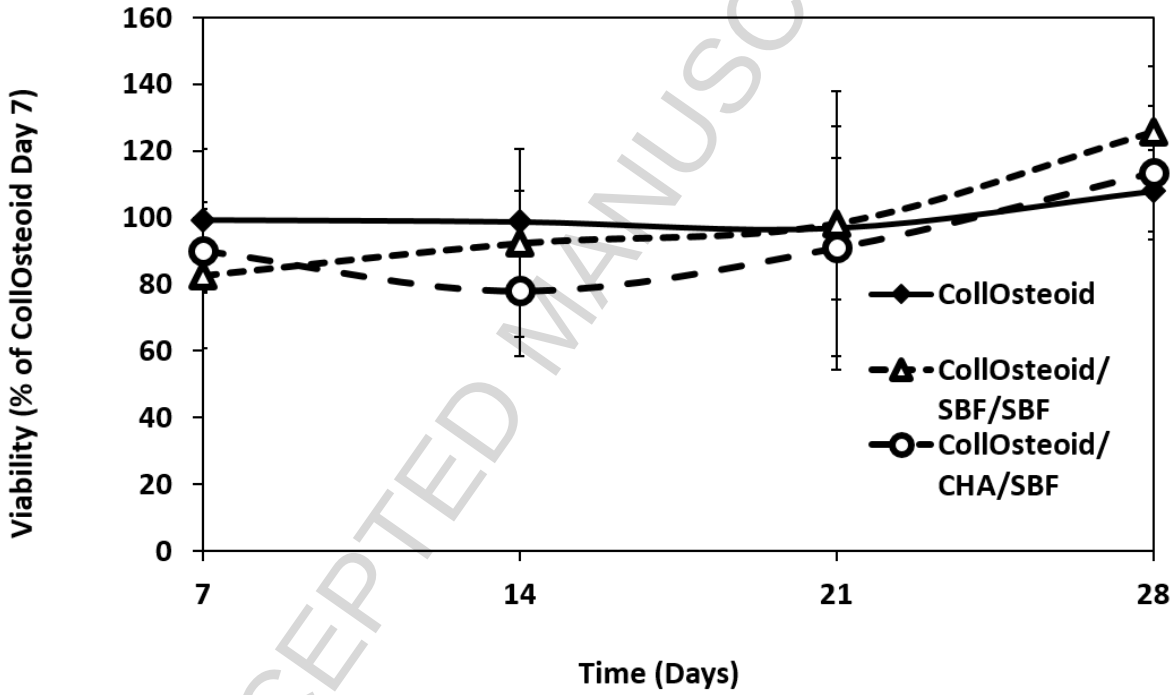

Fig. S6. Study of the cell viability by Alamar Blue metabolic. Osteoblast viability in CollOsteoid (♦), CollOsteoid/SBF/SBF (△) and CollOsteoid/CHA/SBF (o) matrices at days 7, 14, 21 and 28.

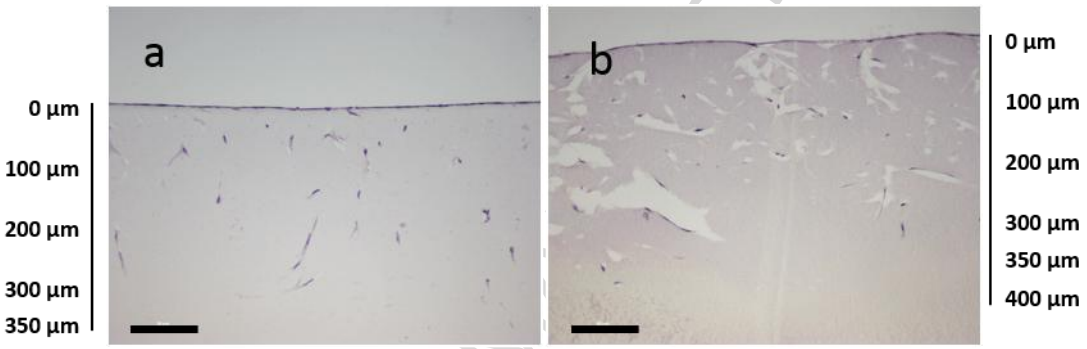

Fig. S7. In-depth osteoblast migration observed in the mineralized matrices. Paraffin sections with Hemalum staining (a) CollOsteoid/SBF/SBF and (b) CollOsteoid/CHA/SBF matrices at day 28 exhibit the longer migration distance of osteoblasts inside the mineralized matrices. Scale bar 100 µm.

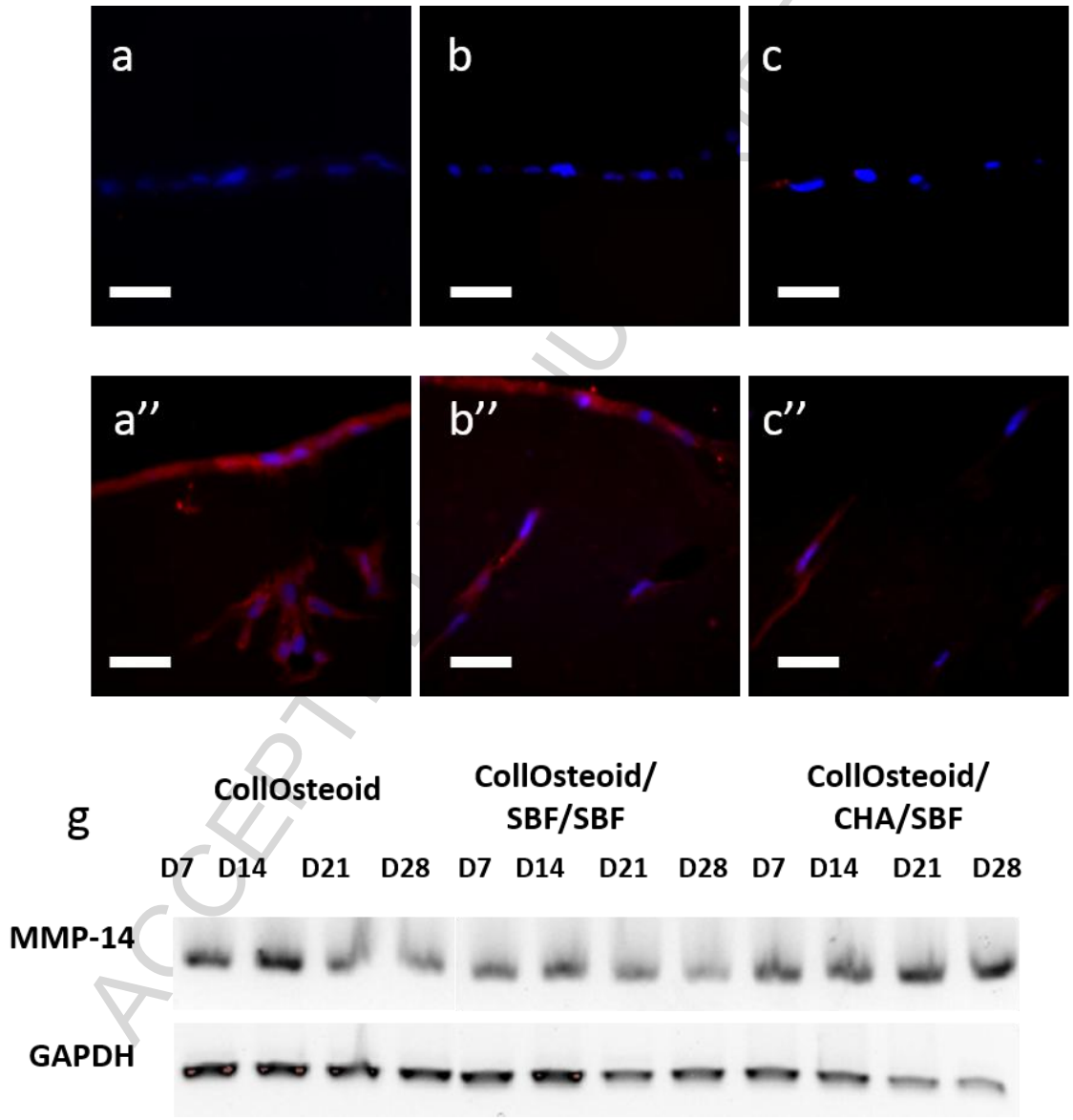

Fig. S8. Matrix Metalloproteinases involved in collagen degradation. MMP-2 is not detected by immunohistochemistry at day 7 (a, b and c) but is observed at day 28 (a'', b'' and c''). Scale bar 50 µm. RT-PCR of MMP-14 shows that this MMP is expressed at all time point in osteoblasts cultivated in all matrices (g).

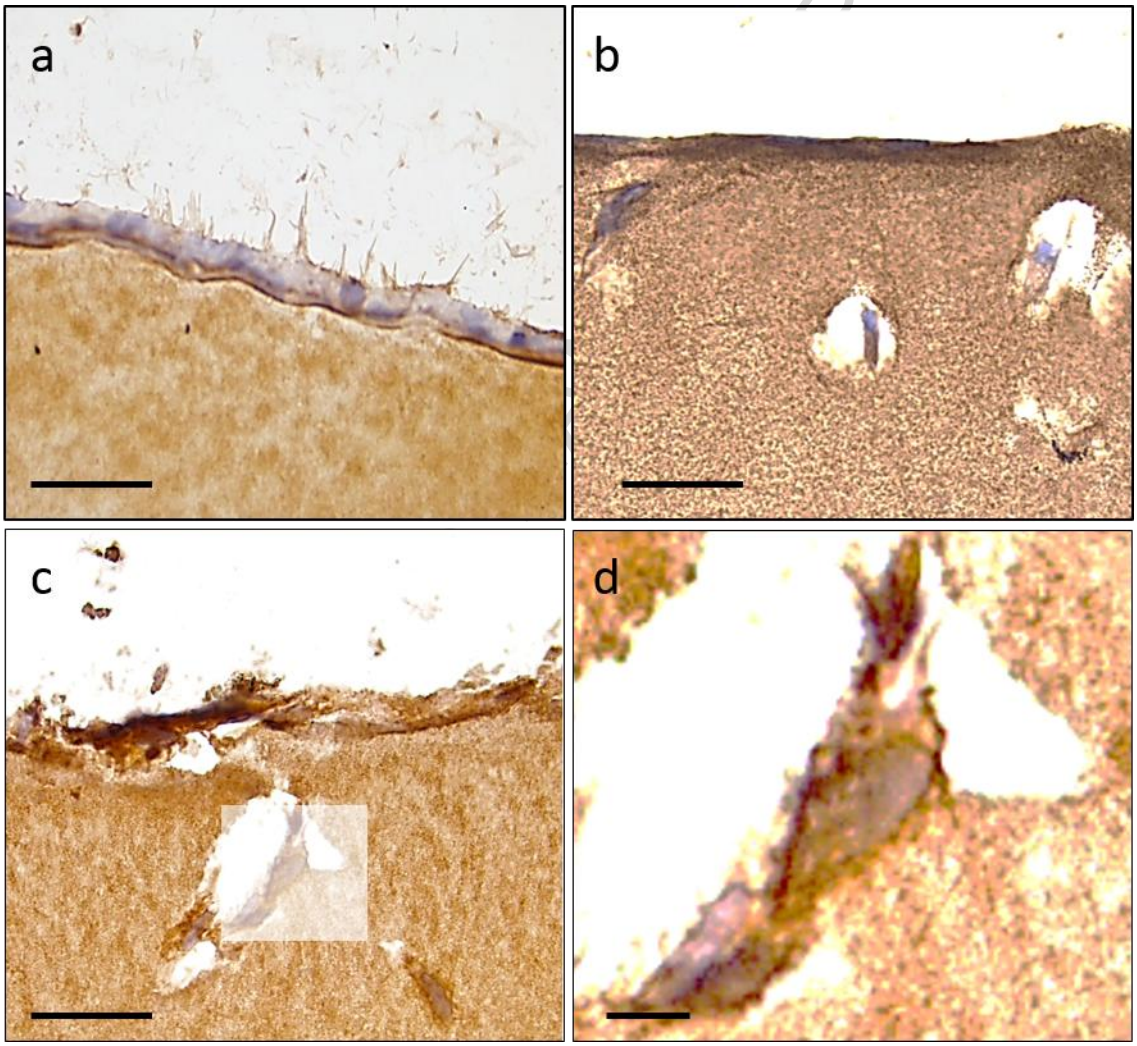

Fig. S9. DMP1 immunodetection. (a) CollOsteoid (b) CollOsteoid/SBF/SBF and (c) CollOsteoid/CHA/SBF. Scale bar 50 µm. The light rectangle in (c) indicates the enlarged section that is shown in (d) where the DMP1 labelling (darkish brown) is more clearly seen. Inset scale bar 10 µm.

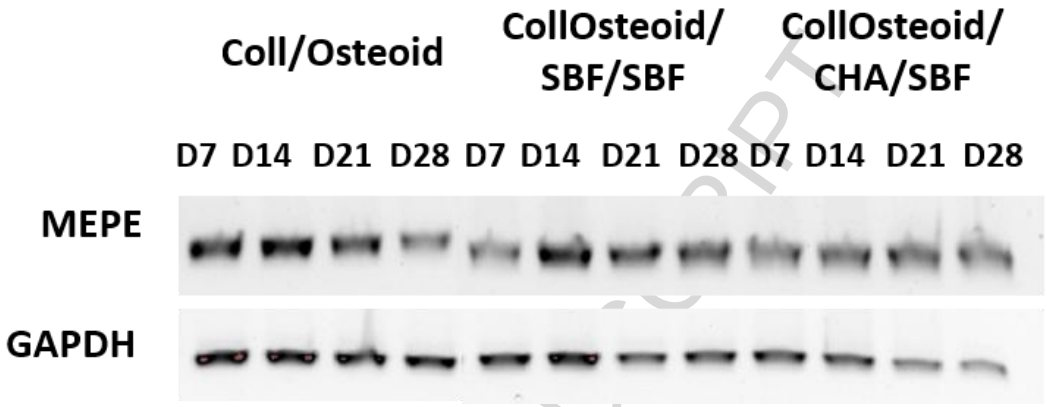

Fig. S10. RT-PCR of MEPE. This gene is expressed by osteoblasts during all the study in all matrices.

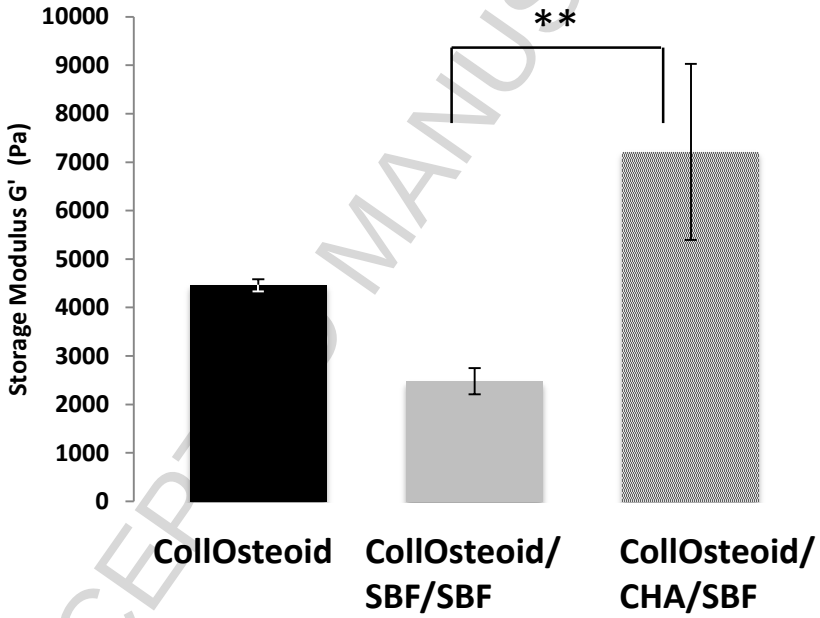

Fig. S11. Mechanical properties of the different matrices assessed by rheology. The Young modulus is 3 times the storage modulus G' measured.

Highlights

- Osteoblasts were cultured on osteoid-like matrices in terms of collagen density, texture and 3D features.
- We used synthetic bone-like apatite platelets in terms of structure and properties.
- Bone apatite appears as a stimulus for osteoblast migration inside the matrix and differentiation into early osteocytes.
- We provide evidence for a new pathway for osteocytogenesis *via* osteoblast migration.
- Our results promise original models to study fundamental questions on biomineralization.